TrpML-mediated astrocyte microdomain Ca^{2+} transients regulate astrocyte-tracheal interactions

Zhiguo Ma and Marc R. Freeman*

Vollum Institute, Oregon Health and Science University, Portland, OR

* correspondence to: freemmar@ohsu.edu

Running title: Astrocyte Ca^{2+} signaling regulates trachea

Abstract

Astrocytes exhibit spatially-restricted near-membrane microdomain Ca^{2+} transients in their fine processes. How these transients are generated and regulate brain function *in vivo* remains unclear. Here we show that *Drosophila* astrocytes exhibit spontaneous, activity-independent microdomain Ca^{2+} transients in their fine processes. Astrocyte microdomain Ca^{2+} transients are mediated by the TRP channel TrpML, stimulated by reactive oxygen species (ROS), and can be enhanced in frequency by the neurotransmitter tyramine via the TyrRII receptor. Interestingly, many astrocyte microdomain Ca^{2+} transients are closely associated with tracheal elements, which dynamically extend filopodia throughout the central nervous system (CNS) to deliver O_2 and regulate gas exchange. Many astrocyte microdomain Ca^{2+} transients are spatio-temporally correlated with the initiation of tracheal filopodial retraction. Loss of TrpML leads to increased tracheal filopodial numbers, growth, and increased CNS ROS. We propose that local ROS production can activate astrocyte microdomain Ca^{2+} transients through TrpML, and that a subset of these microdomain transients promotes tracheal filopodial retraction and in turn modulate CNS gas exchange.

Introduction

Astrocytes exhibit two major types of Ca^{2+} signaling events, whole-cell fluctuations and near membrane microdomain Ca^{2+} transients (Khakh & McCarthy, 2015). Whole-cell transients are coordinated across astrocyte networks and regulated by adrenergic receptor signaling. Emerging data suggests these transients are important for state-dependent changes (Ding et al., 2013; Ma et al., 2016; Paukert et al., 2014; Srinivasan et al., 2015), and involve TRPA1 channels that regulate the insertion of neurotransmitter transporters like GAT-3 into astrocyte membranes to alter neurophysiology (Shigetomi et al., 2011). Whole-cell astrocyte Ca^{2+} transients in the *Drosophila* CNS are also stimulated by the invertebrate equivalents of adrenergic transmitters, octopamine (Oct) and tyramine (Tyr). Octopamine and tyramine stimulate cell-wide astrocyte Ca^{2+} increase through the dual-specificity Octopamine-Tyramine Receptor (Oct-TyrR) and the TRP channel Water witch (Wtrw). This astrocyte-mediated signaling event downstream of octopamine and tyramine is critical for *in vivo* neuromodulation: astrocyte-specific elimination of Oct-TyrR or Wtrw in larvae blocks the ability of octopamine and tyramine to silence downstream dopaminergic neurons, and alters both simple chemosensory behavior and a touch-induced startle response (Ma et al., 2016). Adrenergic regulation of whole-cell astrocyte Ca^{2+} transients is therefore an ancient and broadly conserved feature of metazoan astrocytes.

The mechanisms that generate astrocyte microdomain Ca^{2+} transients are not understood, nor are the precise *in vivo* roles for this type of astrocyte signaling (Bazargani & Attwell, 2016; Khakh & McCarthy, 2015). In mammals, astrocyte microdomain Ca^{2+} transients occur spontaneously, do not require neuronal activity (Nett et al., 2002), depend on extracellular Ca^{2+} (Rungta et al., 2016; Srinivasan et al., 2015), and persist in cultured astrocytes, which has been used to argue they are cell-autonomous (Khakh & McCarthy, 2015; Nett et al., 2002). A recent study described close association of astrocyte microdomain Ca^{2+} transients with mitochondria, and found that pharmacological blockade of the mPTP led to a suppression of transients, while ROS led to an enhancement of transients. These observations led to the proposal that astrocyte microdomain Ca^{2+} transients were generated by opening of the mPTP

during oxidative phosphorylation, perhaps as a means to balance mitochondrial function and ongoing astrocyte support with local metabolic needs (Agarwal et al., 2017).

In this study we report that *Drosophila* astrocytes exhibit spontaneous, activity-independent microdomain Ca^{2+} transients, and show they are mediated by the TRP channel TrpML. Many astrocyte microdomain Ca^{2+} transients are associated with branches and filopodia extending from CNS trachea, an interconnected set of tubules that allow for gas exchange in the larval CNS, and astrocyte microdomain Ca^{2+} transients precede the onset of filopodial retraction. Astrocyte microdomain Ca^{2+} transients are regulated by ROS and loss of TrpML leads to tracheal overgrowth and increased CNS ROS. We propose that one *in vivo* role for tracheal-astrocyte interactions is to regulate CNS gas exchange, with tracheal filopodia-dependent local hyperoxia resulting in increased production of ROS, which gates TrpML to generate local astrocyte microdomain Ca^{2+} transients, ultimately promoting tracheal retraction and reducing local O_2 delivery.

Results

Drosophila astrocytes exhibit microdomain Ca^{2+} transients

To monitor the near membrane Ca^{2+} activity in astrocytes, we expressed myristoylated GCaMP5a (myr-GCaMP5a) in astrocytes using the astrocyte-specific *alrm-Gal4* driver. We acutely dissected 3rd instar larval CNS and live-imaged myr-GCaMP5a signals in the ventral nerve cord (VNC) (Ma et al., 2016). We collected images at the midpoint of the neuropil along the dorsoventral axis for 6 minute time windows (Figure 1A). We found that astrocyte microdomain Ca^{2+} transients exhibited diverse waveforms, with variable durations and frequencies (Figure 1A; Figure 1 – Figure supplement 2 – Video 1). The average full width at half maximum (FWHM) for these Ca^{2+} transients was 5.5±2.26 (mean±SD) seconds (Figure 1B). Microdomain Ca^{2+} transients frequently occurred at the same location, suggesting there are hotspots where microdomains repeatedly occur for a given astrocyte. The majority of foci exhibited 1-3 events during the 6 minute imaging window (Figure 1C), and Ca^{2+} transients at different sites did not exhibit obvious synchrony with one another. We also observed microdomain Ca^{2+} transients of a similar rise-and-fall pattern, although with a slightly shorter duration

(FWHM, 1.7±0.08s, mean±SD) in the astrocytes of intact L1 (1st instar) larvae (Figure 1-Figure Supplement 1A and 1B; Figure 1 – Figure Supplement 3 – Video 2), suggesting the microdomain Ca^{2+} transients in the acute CNS preparations we observed largely reflect *in vivo* astrocyte activity, although with some differences in duration. Blockade of action potential firing with tetrodotoxin did not alter astrocyte microdomain Ca^{2+} transients, although they were eliminated by removal of extracellular Ca^{2+} and were sensitive to the Ca^{2+} channel blocker lanthanum chloride ($LaCl_3$) (Figure 1D), suggesting Ca^{2+} entry from extracellular space is essential for generation of astrocyte microdomain Ca^{2+} transients.

Astrocytes tile with one another and occupy unique spatial domains in the CNS. We sought to determine whether microdomain Ca^{2+} transients spanned astrocyte-astrocyte cell boundaries, or if they appeared only within the domain of single cells. We used a flippable construct expressing either QF or Gal4 under the control of the *alrm* promoter, along with two genetically encoded Ca^{2+} indicators: *QUAS::myr-GCaMP5a* and *UAS::myr-R-GECO1* (Figure 1- Figure Supplement 1C). To confirm both myr-GCaMP5a and myr-R-GECO1 behaved similarly, we first examined double-positive cells and found both can detect the same microdomain Ca^{2+} transients (Figure 1- Figure Supplement 1D), and in cells exclusively expressing one of these two Ca^{2+} indicators there were no differences in the overall frequency of the microdomain Ca^{2+} events detected between these sensors (Figure 1E). We then identified cell boundaries between myr-GCaMP5a/myr-R-GECO1 single-labeled cells, and examined the dynamics of astrocyte microdomains across those boundaries. We observed coincident signaling with myr-GCaMP5a and myr-R-GECO1 (Figure 1E). These data indicate that individual astrocyte microdomain Ca^{2+} transients can span astrocyte-astrocyte borders. Our observations support the notion that astrocyte microdomain Ca^{2+} transients are regulated by extrinsic cues that can simultaneously stimulate two astrocytes, or that astrocyte-astrocyte communication/coupling is sufficient to coordinate very local Ca^{2+} signaling events across neighboring cells.

Astrocyte microdomain Ca^{2+} transients are enhanced by tyramine through TyrRII and mediated by TrpML

To determine whether neurotransmitters were capable of modulating astrocyte microdomain Ca^{2+} transients, we bath applied several neurotransmitters and live-imaged astrocyte microdomain Ca^{2+} events. Application of glutamate, acetylcholine, GABA, or octopamine had no effect on the frequency of astrocyte microdomain Ca^{2+} transients (Figure 2A). In contrast, application of tyramine led to a significant increase in the frequency of these transients by ~40% (Figure 2B). We screened the known receptors for tyramine in *Drosophila* and found that astrocyte-specific depletion of TyrRII blocked the ability of tyramine to increase astrocyte microdomain Ca^{2+} transients. The spontaneous microdomain events were not dependent on the presence of tyramine or octopamine, as mutants that block the production of tyramine and octopamine ($Tdc2^{RO54}$) or octopamine ($T\beta h^{nM18}$) did not significantly alter the frequency of astrocyte microdomain Ca^{2+} transients, nor did mutations in *Oct-TyrR*, which we previously showed was essential for activation of whole-cell Ca^{2+} transients in astrocytes (Figure 2C). These data indicate that while astrocyte microdomain Ca^{2+} transients can be partially enhanced by tyramine through TyrRII, under basal conditions astrocytes do not require tyramine or octopamine for microdomain Ca^{2+} transient activity.

Whole-cell astrocyte transients are regulated by the TRP channel Water witch (Wtrw) (Ma et al., 2016), and astrocyte basal Ca^{2+} levels in mammals are modulated by TrpA1 (Shigetomi et al., 2013). The molecular pathways that generate astrocyte microdomain Ca^{2+} transients have not been identified. We speculated that astrocyte microdomain Ca^{2+} transients might be regulated by one or more of the 13 TRP channels encoded in the *Drosophila* genome. We screened these for potential roles in the regulation of astrocyte microdomain Ca^{2+} transients in animals bearing Trp channel mutations or astrocyte-specific RNAi targeting *trp* family genes. While knockout of 11 of these TRP channels had no effect, we found that microdomain Ca^{2+} events decreased by ~70% to 80% in *trpml* loss-of-function mutants, in both intact 1st instar larvae (Figure 2 - Figure Supplement 1A) and acute CNS preparations from 3rd instar larvae (Figure 2D; Figure 2 – Figure Supplement 2 – Video 1). Astrocyte specific knockdown of *trpml* also reduced microdomain Ca^{2+} events by ~60% (Figure 2D), and expressing a version of myc-tagged TrpML (*trpml-myc*) in astrocytes rescued decreased microdomains in *trpml* mutants (Figure 2E; Figure 2 - Figure Supplement 1B), arguing for a cell

autonomous role of TrpML in regulating astrocyte microdomain Ca^{2+} transients. Although application of tyramine still increased microdomain Ca^{2+} events in *trpml*^{1} mutants, the enhancement above the basal level of spontaneous microdomain Ca^{2+} transients was significantly reduced (Figure 2F), suggesting tyramine enhances microdomains in frequency at least in part via TrpML.

We next examined whether TrpML was essential for tyramine activated Ca^{2+} events in astrocytes cell bodies, and found that tyramine induced comparable Ca^{2+} rise in astrocytes in control and *trpml*^{1} mutants (Figure 2 - Figure Supplement 1C). This argues for a specific role of TrpML in generating microdomain Ca^{2+} transients. While glial cells undergo apoptosis in *trpml* mutant adults (Venkatachalam et al., 2008), astrocyte development appears to be normal at 3rd instar larval stage (Figure 2 - Figure Supplement 1D). Interestingly, *trpml*^{1} mutants exhibit near fully penetrant lethality during later pupal stages as previously reported (Venkatachalam et al., 2008), and we found that expression of *trpml-myc* selectively in astrocytes rescued this lethality (Figure 2 - Figure Supplement 1E), demonstrating that TrpML plays an essential role in astrocytes. The myc-tagged version of TrpML predominantly localized at GFP-Lamp1^{+} endo-lysosomes in astrocytes in both fine astrocytic processes and cell bodies, as well as near the cell membrane (Figure 2 - Figure Supplement 1F). TrpML might therefore execute its regulation of astrocyte microdomains from endo-lysosomes, the plasma membrane, or both.

Previous work has shown that reactive oxygen species (ROS) can activate TrpML (X. Zhang et al., 2016), and astrocyte near membrane Ca^{2+} events in mammals are sensitive to ROS (Agarwal et al., 2017). We therefore assayed the sensitivity of *Drosophila* astrocyte microdomain Ca^{2+} transients to ROS. We observed that bath application of the ROS generator hydrogen peroxide (H_2O_2) led to a TrpML-dependent increase in astrocyte microdomain Ca^{2+} events, while, reciprocally, addition of the antioxidant N-acetyl cysteine completely abolished them (Figure 2G and 2H; Figure 2 – Figure Supplements 3,4 – Videos 2,3). These data indicate that astrocyte microdomain Ca^{2+} transients are mediated by TrpML and are highly sensitive to ROS. Furthermore, our observation that TrpML and Wtrw regulate only microdomain or whole-cell Ca^{2+} events, respectively, demonstrates that astrocyte microdomain Ca^{2+} transients and

whole-cell changes in astrocyte Ca^{2+} are physiologically and genetically distinct signaling events, although adrenergic transmitters (tyramine in *Drosophila* and norepinephrine in mouse) may serve as factors to coordinate their activity.

Astrocyte microdomain Ca^{2+} transients are associated with trachea and precede tracheal filopodia retraction

Mammalian astrocytes make intimate contacts with blood vessels by forming endfeet to allow for gas exchange, uptake of nutrients from blood, and maintenance of the blood brain barrier. Fine astrocyte processes in *Drosophila* infiltrate the CNS neuropil where they associate with neural processes, synapses, and tracheal elements (Freeman, 2015). Tracheal cells serve a similar function to mammalian blood vessels, and their development and morphogenesis are molecularly similar (Ghabrial et al., 2003). Trachea are an interconnected series of gas-filled tubes that penetrate insect tissues, and gas exchange occurs through tracheal cell-tissue interactions (Ghabrial et al., 2003). Interestingly, we observed that half of all astrocyte microdomain Ca^{2+} transients we recorded were closely associated with CNS tracheal elements (Figure 3A). In live preparations where trachea were labeled with myristoylated tdTomato (myr-tdTom) and either Lifeact-GFP to visualize actin or Tubulin-GFP to visualize microtubules, we observed that tracheal branches dynamically extended and retracted actin-rich protrusions that are characteristic of filopodia (Figure 3B), and only very few were stabilized by microtubules (Figure 3 – Figure Supplement 1A). These observations imply tracheal branches dynamically explore their surroundings in the CNS with filopodia.

We classified tracheal filopodia into 4 categories according to different behavior they exhibited during imaging: extension (1.7%), retraction (20.7%), extension and retraction (75.3%), or stationary (2.3%) (Fig 3C). The vast majority of tracheal filopodia dynamically extended and retracted during the imaging window of 6 minutes. We note that those that exhibited only retraction did so very early in the imaging window, which could indicate that we began our imaging after extension had been initiated, however we cannot exclude the possibility that our imaging approach biases tracheal dynamics more toward retraction (e.g. by our imaging procedure generating ROS).

Based on their close association, we explored the potential relationship between tracheal filopodial dynamics and astrocyte microdomain Ca^{2+} transients. Interestingly, 52% of tracheal filopodial tips overlapped, at some point, with an astrocyte microdomain Ca^{2+} transient (Figure 3C). Overlap was defined as the tracheal filopodial tip falling within the maximum size of the domain of the astrocyte Ca^{2+} transient. Moreover, we observed that astrocyte microdomain Ca^{2+} transients preceded retraction events of tracheal filopodia within their domain. The onset of trachea filopodial retraction was tightly correlated with astrocyte microdomain Ca^{2+} peaks (R^2=0.99, Figure 3D-3F; Figure 3 – Figure Supplement 1B; Figure 3 – Figure Supplement 2 – Video 1), with a latency time of 25.9±2.18s. In contrast, the intervals between trachea filopodial extension onset and astrocyte microdomain Ca^{2+} peaks were significantly larger (144.6±11.65s) and more broadly distributed (Figure 3 – Figure Supplement 1C). Correlations between astrocyte microdomains and any changes in tracheal filopodial dynamics were only observed when filopodia overlapped with astrocyte microdomain Ca^{2+} transients. For instance, we found no correlation between extension or retraction of filopodia and nearby non-overlapping astrocyte microdomain Ca^{2+} transients ("bystanders") within an circular area beginning 7.5μm away from filapodial tips and extending outward (Figure 3 – Figure Supplement 1D). We note that 46% of tracheal filopodia were not visibly associated with astrocyte microdomain Ca^{2+} transients. This argues that a large fraction of tracheal filopodia can extend and retract in the absence of local astrocyte microdomain Ca^{2+} signaling. However, we cannot exclude the possibility that astrocyte Ca^{2+} signaling above or below the plane of focus could be modulating the dynamics of these trachea. Together, these observations indicate that a large fraction of astrocyte microdomain Ca^{2+} transients are spatiotemporally correlated with the retraction of adjacent tracheal filopodia.

Blockade of astrocyte microdomain Ca^{2+} transients increases CNS ROS and *trpml* mutants exhibit increased tracheal growth

Based on their spatiotemporal association, we speculated that astrocyte microdomain Ca^{2+} transients promote tracheal filopodial retraction in response to ROS through TrpML. This predicts that loss of these transients would increase tracheal filopodial growth. To

block astrocyte microdomain Ca^{2+} transients we used *trpml*^{1} mutants and labeled tracheal membranes with myr-tdTom. We found in *trpml*^{1} mutants that the overall rate of filopodial extension over time was indeed increased, which resulted in an increase in maximum length of the tracheal filopodia (Figure 4A). The increased filopodial extension rate, but not the maximum length of the filopodia, was phenocopied by knocking down *trpml* selectively in either astrocytes, and to some extent in trachea (Figure 4 – Figure Supplement 1A), arguing that TrpML functions in both astrocytes and trachea to control tracheal filopodial growth. Filopodial retraction rates remained unchanged in *trpml*^{1} mutants, suggesting astrocyte TrpML signaling facilitates tracheal filopodial retraction by suppressing extension. Our model further predicts that stimulating an increased number of astrocyte microdomain Ca^{2+} transients should promote filopodial retraction. To test this idea we bath applied tyramine, which stimulates astrocyte microdomain Ca^{2+} transients. We found tyramine application led to an increase in the percentage of tracheal filopodial retracting versus extending (Figure 4B), further supporting the notion that astrocyte microdomains facilitate filopodial retraction.

To quantify the longer term structural effect of loss of *trpml* (and astrocyte microdomain Ca^{2+} transients), we examined tracheal structure in larval CNS. We first counted the total number of protrusions from a pair of most posterior ganglion trachea (mpgTr) that innervate a few segments from A5 to A8/9 in the ventral nerve cord. We found that mpgTr in the ventral nerve cord in *trpml*^{1} mutants exhibit increased total length compared to those in control animals (Figure 4 – Figure Supplement 1B). We next examined a uniquely identifiable branch of the tracheal system in the larval optic neuropil (LON) (Sprecher et al., 2011). The LON is a simple tissue, composed of only a few dozen neurons and 1~2 tracheal branches that are surrounded by the processes from a single astrocyte (Figure 4 – Figure Supplement 1C). Compared to controls, we found that *trpml*^{1} mutants exhibited an approximate doubling of the number of tracheal branches, and also total filopodia in the LON (Figure 4C). Together these data indicate that TrpML restricts tracheal outgrowth through astrocyte microdomain Ca^{2+} transients.

It is plausible that such an increase in tracheal branches and filopodia might result in excessive O_2 delivery to CNS tissues and result in a hyperoxia. To assay ROS status in the CNS we stained with the ROS indicator dihydroethidium (DHE). In live

preparations of *trpml*^{1} mutants we found a ~3-fold increase in oxidized DHE^{+} puncta, likely in mitochondria (Bindokas et al., 1996), and when we eliminated *trpml* selectively from astrocytes by RNAi, we found a ~2.5-fold increase in oxidized DHE^{+} puncta (Figure 4D). We also validated our DHE staining by a 5-min period of acute pre-treatment with the ROS scavenger NAC, which reduced DHE^{+} puncta in *trpml*^{1} mutants (Figure 4D; Figure 4 – Figure Supplement 1D). These data support the notion that blockade of TrpML signaling, and in turn astrocyte microdomain Ca^{2+} transients, leads to increased ROS in the CNS, perhaps due to excessive O_2 delivery from increased tracheal elements (Figure 4E).

Discussion

Molecules required for the generation of astrocyte microdomain Ca^{2+} transients have remained elusive, it remains unclear how many "types" of microdomain Ca^{2+} exist in astrocytes, and the *in vivo* roles for these transients remain controversial and poorly defined (Agarwal et al., 2017; Bazargani & Attwell, 2016). Our work demonstrates that *Drosophila* astrocyte microdomain Ca^{2+} transients are mediated by the TRP channel TrpML, and can be stimulated by ROS and tyramine through the TyrRII receptor. Unexpectedly, we found that a large fraction of astrocyte microdomain Ca^{2+} transients are closely associated with tracheal elements, precede and are tightly coupled with tracheal filopodial retraction, and that stimulating astrocyte microdomain Ca^{2+} transients with tyramine can promote tracheal filopodial retraction. We propose that one important physiological role for a subset of astrocyte microdomain Ca^{2+} transients is to modulate CNS gas exchange through TrpML and ROS signaling.

Astrocyte microdomain Ca^{2+} transients in *Drosophila* share many features with those observed in mammals (Agarwal et al., 2017; Nett et al., 2002; Srinivasan et al., 2015; Y. V. Zhang et al., 2017). They are spontaneously generated, exhibit diverse waveforms, and appear for the most part asynchronous across astrocyte populations. Their production requires the presence of extracellular Ca^{2+} and they are suppressed by the broad Ca^{2+} channel blocker $LaCl_3$. Our analysis of adjacent astrocytes that are labeled with uniquely identifiable Ca^{2+} indicators (myr-GCaMP5a versus myr-R-GECO1) demonstrated individual astrocyte microdomain Ca^{2+} transients can span astrocyte-

astrocyte boundaries, which might argue for an extrinsic mechanism regulating their production. Alternatively, it might indicate that astrocyte-astrocyte coupling of Ca^{2+} signaling events is strong during their production. Astrocyte microdomain Ca^{2+} transients are not suppressed by blockade of action potentials with tetrodotoxin, suggesting they are not activity dependent, although we also cannot formally rule out a role for spontaneous release of neurotransmitters at synapses.

Based on their persistence in *Tdc2* mutants, which lack tyramine and octopamine in CNS, we conclude that spontaneous astrocyte microdomain Ca^{2+} transients do not require the production of tyramine or octopamine *in vivo*. Nevertheless, and similar to application of norepinephrine to mouse preparations (Agarwal et al., 2017), we found that tyramine was capable of stimulating a partial increase in astrocyte microdomain Ca^{2+} transients, and that to some extent this required the tyramine receptor TyrRII on astrocytes. Why these transients do not require tyramine for their spontaneous production, but can be stimulated by tyramine application, remains unclear, but this adrenergic regulation of astrocyte microdomain Ca^{2+} signaling appears to be a conserved feature in *Drosophila* and mouse. It is possibile that adrenergic regulation may serve as a way to physiologically couple whole cell and microdomain Ca^{2+} transients, as a mechanism to coordinate neuronal activity with astrocyte calcium signaling, or both. The regulation of astrocyte Ca^{2+} signaling *in vivo* by octopamine and tyramine is complex. Tyramine can stimulate increases in whole-cell Ca^{2+} levels in astrocytes through the Oct-TyrR, as does octopamine (Ma et al., 2016), but the latter has no effect in astrocyte microdomain Ca^{2+} transients. Signaling mediated by TyrRII may somehow increase the open probability of TrpML in microdomains in a way that is distinct from whole-cell Ca^{2+} signaling. This is consistent with our observation that TrpML is partially responsible for the tyramine-induced increase in astrocyte microdomain Ca^{2+} transients.

TrpML may exert its effects on astrocytic microdomain Ca^{2+} transients at endo-lysosomes, at the cell cortex, or both (Figure 4E). TrpML is well known to signal in the endo-lysosomal compartment as well as the plasma membrane (Feng et al., 2014). We observed localization of TrpML to endo-lysosomes and the cell surface (or cell cortex) in *Drosophila* astrocytes. TrpML may function in astrocytic endo-lysosomes (e.g. Ca^{2+}

release from these compartments) to indirectly activate Ca^{2+} entry through other cation channels at the cell surface. Alternatively, TrpML might function at the cell surface to directly drive Ca^{2+} entry, or stimulate entry from the extracellular space by other channels, or release form intracellular stores. It is also important to note that while we have assayed Ca^{2+} entry, TrpML is also capable of passing several other cations (Feng et al., 2014), and so its role in regulating astrocyte functions could be mediated by cations in addition to Ca^{2+}.

Astrocyte microdomain Ca^{2+} transients and whole-cell changes in astrocyte Ca^{2+} signaling appear to be distinct, in terms of their regulation by neurotransmitters and the molecular machinery generating each type of event (Agarwal et al., 2017; Bazargani & Attwell, 2016; Srinivasan et al., 2015). In mammals, whole-cell astrocyte Ca^{2+} transients are modulated by norepinephrine, adrenergic receptor signaling, and startle stimuli, while microdomain Ca^{2+} transients are activity-independent, associated with mitochondria and are sensitive to ROS (Agarwal et al., 2017; Ding et al., 2013; Paukert et al., 2014). Similarly, whole-cell transients in *Drosophila* astrocytes are activated by tyramine or octopamine (the invertebrate adrenergic neurotransmitters). We previously showed activates the Oct-TyrR receptor and the TRP channel Waterwitch on astrocytes, and in turn through the adenosine receptor AdoR, mediate many of the physiological and behavioral changes exerted by tyramine and octopamine (Ma et al., 2016). In contrast, microdomain Ca^{2+} transients in astrocytes are not regulated by neural activity, are mediated by TrpML (but not Oct-TyrR or Wtrw) and they are sensitive to ROS.

In mouse, a subset of microdomain Ca^{2+} transients are associated with mitochondria, which have been proposed to serve as a source of ROS, potentially through transient opening of the mPTP (Agarwal et al., 2017). These events may also require mitochondria in *Drosophila*, however the density of mitochondria in astrocyte processes was sufficiently high in our preparations that drawing such a conclusion was not feasible—a single astrocyte microdomain Ca^{2+} transient appears to span domains that include many mitochondria. It is reasonable to speculate that astrocyte microdomain Ca^{2+} transients across species are to a significant extent functionally distinct from whole-cell fluctuations, and that they play a role in coupling astrocyte signaling with tracheal/vasculature dynamics or other metabolic changes occurring in

astrocytic mitochondria (Agarwal et al., 2017). Multiple distinct functional roles for astrocyte microdomain Ca^{2+} signaling (i.e. in tracheal regulation versus metabolism) could explain why although only half of all observed astrocyte microdomain Ca^{2+} transients are associated with tracheal filopodia, all appear to be potently regulated by ROS. Perhaps the remaining half of astrocyte microdomain Ca^{2+} transients not associated with trachea are responding to mitochondria-based metabolic needs through ROS signaling. Finally, approximately half of tracheal filopodia we observed were not visibly associated with astrocyte microdomain Ca^{2+} transients, yet they were able to extend and retract. This argues that other mechanisms exist to modulate tracheal dynamics in the CNS and astrocyte microdomain Ca^{2+} transients only represent one regulatory mechanism.

Maintaining a healthy, spatiotemporally regulated normoxic environment to prevent either hypoxia or hyperoxia in CNS is an enormous and ongoing challenge, as the O_2-consuming metabolism is thought to fluctuate vigorously in response to neural activity. The close association of astrocyte microdomain Ca^{2+} transients with trachea, the larval breathing apparatus, and with tracheal retraction in particular, suggests a role in modulating CNS gas exchange. Increase in O_2 delivery to tissues can lead to hyperoxia and elevated production of ROS. TrpML has recently been found to be a ROS sensor (X. Zhang et al., 2016), which would allow for a simple mechanism for ROS-mediated activation of TrpML downstream of increased O_2 delivery. Consistent with such a role in regulation of gas exchange, we found an increase in ROS in the CNS of *trpml* mutants, and we demonstrated that bath application of tyramine to stimulate astrocyte microdomain Ca^{2+} transients was sufficient to promote tracheal filopodial retraction. Together our data support a model (Figure 4E) where a subset of TrpML-mediated microdomain Ca^{2+} transients in astrocytes facilitate tracheal retraction, likely in conjuction with TrpML in trachea. Complete loss of TrpML led to an increase in tracheal growth (e.g. an increased vascularization of neural tissues), which argues that astrocyte-tracheal signaling through TrpML can regulate long term structural changes in the tracheal morphology. Based on these findings, we propose that an important role for a subset of astrocyte microdomain Ca^{2+} transients in the larval CNS is to coordinate gas

exchange through regulation of tracheal dynamics, thereby balancing O_2 delivery/CO_2 removal according to local metabolic needs.

Materials and Methods

Key Resources Table				
Reagent type (species) or resource	**Designation**	**Source or reference**	**Identifiers**	**Additional information**
genetic reagent *(D. melanogaster)*	*trpml*^{1}	Bloomington Stock Center	BDSC: 28992	FlyBase symbol: *w*^{1118}*; Trpml*^{1}
genetic reagent *(D. melanogaster)*	*trpml*^{2}	Bloomington Stock Center	BDSC: 42230	FlyBase symbol: *w*; Trpml*^{2}*/TM6B, Tb*^{1}
genetic reagent *(D. melanogaster)*	*trpml*^{JF01239}	Bloomington Stock Center	BDSC: 31294	FlyBase symbol: *y*^{1} *v*^{1}*; P{TRiP.JF01239}attP2*
genetic reagent *(D. melanogaster)*	*tyrR*^{JF01878}	Bloomington Stock Center	BDSC: 25857	FlyBase symbol: *y*^{1} *v*^{1}*; P{TRiP.JF01878}attP2*
genetic reagent *(D. melanogaster)*	*tyrRII*^{JF02749}	Bloomington Stock Center	BDSC: 27670	FlyBase symbol: *y*^{1} *v*^{1}*; P{TRiP.JF02749}attP2*
genetic reagent *(D. melanogaster)*	*trpA1*^{1}	Bloomington Stock Center	BDSC: 36342	FlyBase symbol: *TI{TI}TrpA1*^{1}
genetic reagent *(D. melanogaster)*	*trpm*^{2}	Bloomington Stock Center	BDSC: 35527	FlyBase symbol: *w*; TI{TI}Trpm*^{2}*/CyO*
genetic reagent *(D. melanogaster)*	*nompC*^{3}	Bloomington Stock Center	BDSC: 42258	FlyBase symbol: *nompC*^{3} *cn*^{1} *bw*^{1}*/CyO*
genetic reagent *(D. melanogaster)*	*trp*^{1}	Bloomington Stock Center	BDSC: 5692	FlyBase symbol: *trp*^{1}
genetic reagent *(D. melanogaster)*	*trpl*^{302}	Bloomington Stock Center	BDSC: 31433	FlyBase symbol: *cn*^{1} *trpl*^{302} *bw*^{1}
genetic reagent *(D. melanogaster)*	*pkd2*^{1}	Bloomington Stock Center	BDSC: 24495	FlyBase symbol: *w*^{1118}*; Pkd2*^{1}*/CyO*
genetic reagent *(D. melanogaster)*	*trpγ*^{JF01244}	Bloomington Stock Center	BDSC: 31299	FlyBase symbol: *y*^{1} *v*^{1}*; P{TRiP.JF01244}attP2*
genetic reagent *(D. melanogaster)*	*pyx*^{JF01242}	Bloomington Stock	BDSC: 31297	FlyBase symbol: *y*^{1} *v*^{1}*;*

		Center		*P{TRiP.JF01242}attP2*
genetic reagent *(D. melanogaster)*	*btl-Gal4*	Bloomington Stock Center	BDSC: 8807	FlyBase symbol: *W*; P{GAL4-btl.S}2, P{UASp-Act5C.T:GFP}2/CyO, P{lacZ.w+}276. UASp-Act5C.T:GFP* was replaced with 10XUAS-IVS-myr::tdTomato by recombination in this paper.
genetic reagent *(D. melanogaster)*	*UAS-Lifeact-GFP*	Bloomington Stock Center	BDSC: 57326	FlyBase symbol: *w*; P{UAS-Lifeact.GFP.W}3*
genetic reagent *(D. melanogaster)*	*UASp-αTub-GFP*	Bloomington Stock Center	BDSC: 7373	FlyBase symbol: *w*; P{UASp-GFPS65C-αTub84B}3/TM3, Sb*^{1}
genetic reagent *(D. melanogaster)*	*10XUAS-IVS-myr::tdTomato*	Bloomington Stock Center	BDSC: 32222	FlyBase symbol: *w*; P{10XUAS-IVS-myr::tdTomato}attP40*
genetic reagent *(D. melanogaster)*	*UAS-trpml-myc*	Bloomington Stock Center	BDSC: 57372	FlyBase symbol: *w*; P{UAS-Trpml.MYC}3, Trpml*^{1}*/TM6B, Tb*^{1}*
genetic reagent *(D. melanogaster)*	*5XUAS-trpml-GCaMP5g*	Bloomington Stock Center	BDSC: 80066	FlyBase symbol: *y*^{1} *w*; PBac{5XUAS-Trpml::GCaMP5G}VK00033*
genetic reagent *(D. melanogaster)*	*UAS-GFP-Lamp1*	Bloomington Stock Center	BDSC: 42714	FlyBase symbol: *w*; P{UAS-GFP-LAMP}2; P{nSyb-GAL4.S}3/T(2;3)TSTL, CyO: TM6B, Tb*^{1}*
genetic reagent *(D. melanogaster)*	*Oct-TyrR*^{hono}	Kyoto Stock Center (DGRC)	BDSC: 109038	FlyBase symbol: *w*^{1118}*; P{lwB}Oct-TyrR*^{hono}*
genetic reagent *(D. melanogaster)*	*btl-LexA*	Roy et al., 2014		
genetic reagent *(D. melanogaster)*	*nompC*^{4}	Walker et al., 2000		
genetic reagent *(D. melanogaster)*	*painless*^{70}	Im et al., 2015		
genetic reagent *(D. melanogaster)*	*nan*^{36a}	Kim et al., 2003		

genetic reagent *(D. melanogaster)*	*wtrw*^{ex}	Kim et al., 2010		
genetic reagent *(D. melanogaster)*	*Tdc2*^{RO54}	Cole et al., 2005		
genetic reagent *(D. melanogaster)*	*Tβh*^{nM18}	Monastirioti et al., 1996		
genetic reagent *(D. melanogaster)*	*alrm-Gal4*	Doherty et al., 2009		
genetic reagent *(D. melanogaster)*	*alrm>QF>Gal4*	Stork et al., 2014		
genetic reagent *(D. melanogaster)*	*repo-FLPase*	Stork et al., 2014		
genetic reagent *(D. melanogaster)*	*alrm-LexA::GAD*	Stork et al., 2014		
genetic reagent *(D. melanogaster)*	*UAS-myr::GCaMP5a*	This paper		transgenic flies harboring *UAS-myr::GCaMP5a*
genetic reagent *(D. melanogaster)*	*UAS-myr::R-GECO1*	This paper		transgenic flies harboring *UAS-myr::R-GECO1*
genetic reagent *(D. melanogaster)*	*QUAS-myr::GCaMP5a*	This paper		transgenic flies harboring *QUAS-myr::GCaMP5a*
genetic reagent *(D. melanogaster)*	*13XLexAop2-myr::GCaMP6s*	This paper		transgenic flies harboring *13XLexAop2-myr::GCaMP6s*
antibody	mouse monoclonal anti-Brp	DSHB	Cat# nc82	1:50
antibody	mouse monoclonal anti-c-Myc	DSHB	Cat# 9E10	1:100
chemical compound, drug	tetrodotoxin	Tocris	Cat# 1078	1μM
chemical compound, drug	lanthanum chloride	Sigma-Aldrich	Cat# 211605	0.1mM, 1mM
chemical compound, drug	acetylcholine	Sigma-Aldrich	Cat# A6625	2.5mM
chemical compound, drug	γ-aminobutyric acid (GABA)	Sigma-Aldrich	Cat# A2129	2.5mM
chemical compound, drug	glutamate	Sigma-Aldrich	Cat# G1626	2.5mM
chemical	tyramine	Sigma-	Cat# T90344	2.5mM

compound, drug		Aldrich		
chemical compound, drug	octopamine	Sigma-Aldrich	Cat# O0250	2.5mM
chemical compound, drug	N-acetyl cysteine	Sigma-Aldrich	Cat# A7250	2.5mM
chemical compound, drug	hydrogen peroxide	Sigma-Aldrich	Cat# H1009	0.1mM
chemical compound, drug	halocarbon oil 27	Sigma-Aldrich	Cat# H8773	
chemical compound, drug	dihydroethidium (DHE)	Sigma-Aldrich	Cat# 309800	30µM
recombinant DNA reagent	pUAST-myr::GCaMP5a	This paper	Fly germline transformation plasmid	GCaMP5a DNA with myristoylation sequence fused at the 5' end
recombinant DNA reagent	pQUAST-myr::GCaMP5a	This paper	Fly germline transformation plasmid	GCaMP5a DNA with myristoylation sequence fused at the 5' end
recombinant DNA reagent	pUAST-myr::R-GECO1	This paper	Fly germline transformation plasmid	R-GECO1 DNA with myristoylation sequence fused at the 5' end
recombinant DNA reagent	pJFRC19-13XLexAop2-IVS-myr::GCaMP6s	This paper	Fly germline transformation plasmid	GCaMP6s DNA with myristoylation sequence fused at the 5' end
software, algorithm	Volocity	PerkinElmer, Inc.	http://www.perkinelmer.com/lab-products-and-services/cellular-imaging/performing-advanced-image-data-analysis.html	
software, algorithm	Slidebook	Intelligent Imaging Innovations, Inc.	https://www.intelligent-imaging.com/slidebook	
software, algorithm	Fiji	Schindelin et al., 2012	https://fiji.sc/	

software, algorithm	Graphpad Prism 7	GraphPad software	https://www.graphpad.com/scientific-software/prism/	
software, algorithm	Igor Pro	WaveMetrics, Inc.	https://www.wavemetrics.com/products/igorpro	
software, algorithm	AQuA	Wang et al., 2019	https://github.com/yu-lab-vt/AQuA#fiji-plugin	

Drosophila stocks and husbandry

All larvae/flies were cultured in cornmeal food at 25 ℃ under 12 hour/12 hour dark/light cycles. Female larvae were used for all experiments unless otherwise stated. The specific developmental stages studied in each experiment are indicated in the following Method details. *Drosophila* strains used include: Bloomington stock center *trpml*^{1} (28992), *trpml*^{2} (42230), *trpml*^{JF01239} (31294), *tyrR*^{JF01878} (25857), *tyrRII*^{JF02749} (27670), *trpA1*^{1} (36342), *trpm*^{2} (35527), *nompC*^{3} (42258), *trp*^{1} (5692), *trpl*^{302} (31433), *pkd2*^{1} (24495), *trpγ*^{JF01244} (31299), *pyx*^{JF01242} (31297), *btl-Gal4* (8807), *UAS-Lifeact-GFP* (57326), *UASp-αTub-GFP* (7373), *10XUAS-IVS-myr::tdTomato* (32222), *UAS-trpml-myc* (57372), *UAS-GFP-Lamp1* (42714). *Oct-TyrR*^{hono} (Nagaya et al., 2002), *nompC*^{4} (Walker et al., 2000), *painless*^{70} (Im et al., 2015), *nan*^{36a} (J. Kim et al., 2003), *wtrw*^{ex} (S. H. Kim et al., 2010), *Tdc2*^{RO54} (Cole et al., 2005), *Tβh*^{nM18} (Monastirioti et al., 1996), *alrm-Gal4*(Doherty et al., 2009), *alrm>QF>Gal4*, *repo-FLPase*, *alrm-LexA::GAD* (Stork et al., 2014), *btl-LexA* (Roy et al., 2014), *5XUAS-trpml-GCaMP5g* (Wong et al., 2017). *UAS-myr::GCaMP5a*, *UAS-myr::R-GECO1*, *QUAS-myr::GCaMP5a*, *13XLexAop2-myr::GCaMP6s* flies were generated in this study.

Constructs and transgenic flies

The full-length ORFs of GCaMP5a, R-GECO1, GCaMP6s with an in-frame DNA fragment encoding the myristoylation signal peptide at 5'-end were cloned into vectors pUAST, pQUAST, pJFRC19 (harboring *13XLexAop2-IVS*, referring to the plasmid Addgene Cat# 26224) to generate constructs *pUAST-myr::GCaMP5a*, *pQUAST-*

myr::GCaMP5a, *pUAST-myr::R-GECO1*, *pJFRC19-13XLexAop2-IVS-myr::GCaMP6s* for injection. The transgenic flies were injected and recovered by Rainbow Transgenic Flies, Inc. (California).

Ca^{2+} imaging and data analysis

Ca^{2+} imaging in intact larvae: the 1st instar larva expressing myr-GCaMP5a in astrocytes (25℃, 24-32 hours after egg laying) was sandwiched in 30µl halocarbon oil 27 (Cat# H8773, Sigma-Aldrich) between a slide and a 22 X 22mm coverslip (Cat# 1404-15, Globe Scientific Inc.), then a 3min time-lapse video was taken immediately on a spinning disk confocal microscope equipped with a 40X oil immersion objective.

CNS dissection from early 3rd instar larvae expressing myr-GCaMP5a in astrocytes (larval density ~100, 25℃, 76-84 hours after egg laying) was performed in the imaging buffer (pH7.2) containing 110mM NaCl, 5.4mM KCl, 0.3mM $CaCl_2$, 0.8mM $MgCl_2$, 10mM D-glucose, 10mM HEPES, the CNS was immediately transferred to a silicone coated petri dish, immersed in 100µl imaging buffer (1.2mM $CaCl_2$), and immobilized gently by sticking the attached nerves onto the silicone surface with forceps. The petri dish then was placed on the stage of a spinning disk confocal microscope equipped with a 40X water dipping objective. The focal plane was fixed around where most of the dorsal lateral astrocytes start to appear in the field of view. After 4min acclimation and stabilization, a 6min movie (excitation channel, 488nm. exposure time, 300ms. single focal plane) was taken for analysis. The 488nm and 516nm channels were alternated for imaging both the microdomain Ca^{2+} transients in astrocytes and the dynamics of tracheal filopodia. To keep the tracheal filopodia in focus during the course of extension and retraction, images spanning 5µM in z depth were taken.

The frequency (the number of microdomain Ca^{2+} transients per minute) of microdomain Ca^{2+} transients in each preparation was initially quantified as follows: a 100µm X 100µm window was cropped from each movie and resulted in 9 smaller, side-to-side 100pixel X 100pixel windows (line drawing over movies) in which the number of microdomain Ca^{2+} transients was counted manually. The total number of microdomain Ca^{2+} transients in each preparation (100µm X 100µm) was acquired by adding up all the numbers counted in these 9 100pixel X 100pixel windows. The cutoff for defining a Ca^{2+}

transient is 5% change in delta F/F_0, which is evaluated by *post hoc* calculations after manually selecting active events. After the automatic Ca^{2+} signal analysis software Astrocyte Quantitative Analysis (AQuA)(Wang et al., 2019) became publicly available, we also compared our initial datasets of the dissected CNS from wildtype 3rd instar larvae using the above manual method to the ones obtained through AQuA (Manual vs AQuA-Source Data 8), and we didn't find a significant difference (manual: 16.7±3.69 versus AQuA: 19.8±3.02, p=0.53). The intensity of microdomain Ca^{2+} transients was measured with software Volocity (PerkinElmer, Inc.), and the amplitude of microdomain Ca^{2+} transients was defined by $(F_t-F_0)/F_0$ (t=0,1,2…40, the peak amplitude was designated at t=20, delta F= F_t-F_0) as percentage. The full width at half maximum (FWHM) of astrocyte microdomains was acquired using software Igor Pro (WaveMetrics, Inc.)

For bath application of compounds, halfway through the 6min imaging window (~ 3min), 100µl imaging buffer (1.2mM Ca^{2+}) containing drugs (2X final concentration) was directly applied onto the preparations, then imaging continued for another 3min. The chemicals used for bath application experiments include: Tocris, tetrodotoxin (1µM, Cat# 1078). Sigma-Aldrich, lanthanum chloride ($LaCl_3$, Cat# 211605), acetylcholine (2.5mM, Cat# A6625), γ-aminobutyric acid (GABA, 2.5mM, Cat# A2129), glutamate (2.5mM, Cat# G1626), tyramine (2.5mM, Cat# T90344), octopamine (2.5mM, Cat# O0250), N-acetyl cysteine (NAC, 2.5mM, Cat# A7250), hydrogen peroxide (H_2O_2, 0.1mM, Cat# H1009).

Immunostaining and tracheal branch tracing

The CNS dissected in PBS from 3rd instar larvae (larval density ~100, 25℃, 100-108 hours after egg laying) was immediately transferred in 4% formaldehyde for fixation for 20min (for co-staining with tracheal filopodia, the dissection was performed in the imaging buffer with 0.3mM Ca^{2+}, and the CNS preparations were incubated in the imaging buffer with 1.2mM Ca^{2+} for 10min before 4% formaldehyde fixation). Washing in PBS for 3X 10min. Permeabilization in PBS + 0.3% Triton X-100 for 2 hours. Primary antibody (1:50 anti-Brp, DSHB, Cat# nc82 in PBS + 0.1% Triton X-100) incubation at 4 ℃ for ~72 hours. Secondary antibody incubation at room temperature for ~2 hours.

Tracheal branches in ventral nerve cord were illuminated with 408nm laser light and emitting autofluorescence was imaged. Each individual branch was then traced manually with Simple Neurite Tracer (Fiji).

Reactive oxygen species detection by DHE (dihydroethidium) staining

The CNS preparations from 3rd instar larvae (larval density ~100, 25℃, 100-108 hours after egg laying) were made exactly in the same way for Ca^{2+} imaging. Incubation in 100µl imaging buffer (1.2mM Ca^{2+}) containing 30µM DHE for 8min before imaging (30µm in z depth, starting from the very dorsal side, was taken). The puncta were automatically counted by the segmentation tool in Slidebook.

Statistics

All statistics were performed in Graphpad. No data were excluded for analyses. 2-3 replications were successfully performed for each experiment. Comparison between groups was tested by one-way ANOVA with Tukey's *post hoc* tests, or unpaired t-test. Comparison within groups was tested by paired t-test. $p<0.05$ was considered statistically significant. * $p<0.05$, ** $p<0.01$.

Data Availability

Source data for Figure 1C-1E; Figure 2A-2H; Figure 3E and 3F; Figure 4A-4D; Figure 2 - Figure Supplement 1A-1C, 1E; Figure 3 - Figure Supplement 1D; Figure 4 – Figure Supplement 1A-1B, 1D are included. All other source data is also available on request.

Acknowledgments

We thank Bloomington Stock Center, Kyoto Stock Center, Drs. C.S. Zuker, T.B. Kornberg, C. Montell, J. Hirsh and M. Monastirioti for providing flies. We thank A. Sheehan for making constructs. We thank Freeman lab members for feedback on the manuscript. This work was supported by NIH RO1 NS053538 (to MRF) and OHSU.

Declaration of Interests

The authors declare no competing interests.

552 **Figure Legends**

553

554 **Figure 1. Characterization of microdomain Ca^{2+} transients in *Drosophila***
555 **astrocytes.**

556 (**A**) Schematic of larval CNS (white area, neuropil; gray, cortex). An imaging area
557 showing membrane tethered myr-GCaMP5a (green) in astrocytes, in which
558 microdomain Ca^{2+} transients during 6 min were maximally projected. Traces of 8
559 individual ROIs microdomains (right, a-h) are shown over the entire 6 min window.
560 Pseudocolor grayscale of Ca^{2+} signals (bottom left), grayscale values ranging from 0 to
561 255 (scale bars, 20μm). Representative time-lapse images (bottom right) of two
562 indicated microdomain Ca^{2+} transients in 2 ROIs (1, 2). (**B**) Superimposed traces of
563 individual microdomain Ca^{2+} transients and an average with its full width at half
564 maximum (FWHM, mean±SD). (**C**) Histogram showing the distribution of recurrent
565 microdomain Ca^{2+} transients at same ROIs. (**D**) Responses of microdomain Ca^{2+}
566 transients to tetrodotoxin, 0 extracellular Ca^{2+} and $LaCl_3$ (n=6, mean±SEM, one-way
567 ANOVA). (**E**) 2-color Ca^{2+} imaging in neighboring astrocytes. In presence of the flippase
568 *repo-FLP*, myr-GCaMP5a expressing astrocytes switch to express myr-R-GECO1,
569 resulting in 3 types of astrocytes: myr-GCaMP5a^{+} (green), myr-R-GECO1^{+} (red),
570 expressing both indicators (orange) (scale bar, 20μm). Quantification is from Ca^{2+}
571 imaging of myr-GCaMP5a and myr-R-GECO1 that were exclusively expressed in
572 adjacent astrocytes (n=3, unpaired t-test). Time-lapse images and superimposed traces
573 of representative microdomain Ca^{2+} transients at 2 juxtaposed ROIs between myr-
574 GCaMP5a and myr-R-GECO1 expressing astrocytes. See source data Figure 1 -
575 Source Data 1.

576

577 **Figure 1 - Figure supplement 1. Spontaneous astrocyte microdomain Ca^{2+}**
578 **transients in larvae.**

579 (**A**) Astrocytes expressing myr-GCaMP5a in the ventral nerve cord of 1st instar larvae.
580 Traces of 8 representative microdomain Ca^{2+} transients. (**B**) Superimposed traces of

581 individual microdomain Ca^{2+} transients and an average showing its full width at half
582 maximum (FWHM, mean±SD). (**C**) Schematic of inducing 2-color Ca^{2+} indicators
583 mosaic expression in neighboring astrocytes (green, red, orange). (**D**) Two
584 representative microdomain Ca^{2+} transients in dual-labeled myr-GCaMP5a/myr-R-
585 GECO1 astrocytes. Note that both myr-GCaMP5a and myr-R-GECO1 exhibit similar
586 dynamics in the same astrocyte.
587

588 **Figure 2. Astrocyte microdomain Ca^{2+} transients are genetically distinct from**
589 **soma transients and require TrpML.**

590 (**A**) Responses of microdomain Ca^{2+} transients (frequency) to glutamate (Glu),
591 acetylcholine (Ach), γ-aminobutyric acid (Gaba), tyramine (Tyr), octopamine (Oct) in
592 presence of tetrodotoxin. (**B**) Effect of tyramine on Ca^{2+} transient frequency in
593 genotypes indicated. *Oct-TyrR* mutants, and astrocyte-specific (*alrm>*) expression of
594 RNAis to TyrR or TyrRII (in A and B, n=6, mean±SEM, paired t-test). (**C**) Quantification
595 of microdomain Ca^{2+} transients in $Tdc2^{RO54}$, $T\beta h^{nM18}$ or $Oct\text{-}TyrR^{hono}$ mutants (n=6,
596 mean±SEM, one-way ANOVA). (**D**) Maximally projected astrocyte microdomain Ca^{2+}
597 transients during 6min in control, $trpml^{1}$ mutants, and astrocyte-specific $trpml^{RNAi}$ (in
598 pseudocolor, grayscale values ranging from 0 to 255. scale bar, 20μm). Quantification of
599 microdomain Ca^{2+} transients in mutants (loss-of-function mutations or astrocyte specific
600 RNAi driven by *alrm-Gal4*) of genes encoding TRP family ion channels (n=6,
601 mean±SEM, one-way ANOVA). (**E**) *trpml-myc* expression in astrocytes rescues
602 microdomain Ca^{2+} transients in $trpml^{1}$ mutants (n=6, mean±SEM, one-way ANOVA). (**F**)
603 Effect of tyramine treatment on controls and $trpml^{1}$ mutants (n=6, mean±SEM, one-way
604 ANOVA. within groups, paired t-test). Right panel, increase in transients by tyramine
605 (subtracting the basal included) in control and $trpml^{1}$ mutants. (**G**) Application of the
606 antioxidant N-acetyl cysteine (NAC) or H_2O_2 to the larval CNS. (for F and G n=6,
607 mean±SEM, across groups, one-way ANOVA; within groups, paired t-test; -, + indicate
608 pre-, post-delivery). (**H**) H_2O_2 application to control and *trpml* mutants shows that H_2O_2-
609 dependent increases require TrpML. See source data Figure 2 - Source Data 1.

610

611 **Figure 2 - Figure Supplement 1. Astrocyte microdomain Ca^{2+} transients require**
612 **TrpML.**

613 (**A**) Quantification of microdomain Ca^{2+} transients in intact control and *trpml*^{1} mutant
614 larvae at 1st instar stage (n=6, mean±SEM, t-test). (**B**) Average amplitude of
615 microdomain Ca^{2+} transients in genotypes as indicated (n=6, mean±SEM, one-way
616 ANOVA). (**C**) Tyramine induced soma Ca^{2+} rise measured in GCaMP6s intensity (n=70-
617 73 cells from 6 larval CNS in each genotype, mean±SEM, t-test). (**D**) Gross astrocyte
618 morphology in control and *trpml*^{1}*.* (**E**) *trpml*^{1} mutant larvae with *trpml-myc* expression in
619 astrocytes survived to adulthood (n=3, each n contains 20-40 larvae, mean±SEM, t-
620 test). (**F**) Double-labeling TrpML-MYC with a marker for cell membrane (mCD8-GFP) or
621 lysosomes (GFP-Lamp1). Dash lines, cell bodies. Arrows, TrpML-MYC/GFP-Lamp1
622 colocalization. See source data Figure 2 - Source Data 2.

623

624 **Figure 3. Astrocyte microdomain Ca^{2+} transients are associated with tracheal**
625 **branches and precede retraction onset of tracheal filopodia.**

626 (**A**) Astrocyte microdomain Ca^{2+} transients (green) overlap with tracheal branches (red)
627 (scale bar, 20μm). (**B**) Tracheal branches extend and retract F-actin containing filopodia.
628 Asterisks, myr-tdTomato labeled filopodia; Arrows, Lifeact-GFP labeled F-actin (scale
629 bar, 10μm). (**C**) Categorization of tracheal filopodia across the entire population
630 (extension, retraction, extension and retraction, or stationary). w/Ca^{2+} indicates tracheal
631 filopodia extended into an astrocyte microdomain Ca^{2+} transient; w/o Ca^{2+} indicates no
632 visible astrocyte microdomain Ca^{2+} transient was observed. (**D**) Time-lapse images and
633 superimposed traces (green trace, myr-GCaMP5a in astrocytes expressed as dF/F_0; red
634 trace, myr-tdTomato in tracheal filopodia expressed as length) of 3 pairs (p1, p2, p3) of
635 tracheal filopodia and astrocyte microdomain Ca^{2+} transients (in pseudocolor, grayscale
636 values ranging from 0 to 255. scale bar, 10μm). Vertical dash lines, timepoints when
637 tracheal filopodia enter astrocyte Ca^{2+} microdomains. Blue boxes, time windows
638 astrocyte microdomain Ca^{2+} transients persist after tracheal filopodia enter. Note that

639 prior to entering the astrocyte Ca^{2+} microdomain, tracheal filopodial extension is not
640 coupled to increases in astrocyte Ca^{2+}, but after entry, increased astrocyte Ca^{2+} is
641 strongly correlated with tracheal filopodial retraction. (**E**) Temporal correlation between
642 onset of filopodia retraction and timing of peak astrocyte microdomain Ca^{2+} transients in
643 seconds (n=61 filopodia from Extension & Retraction pool). (**F**) Time intervals between
644 astrocyte microdomain Ca^{2+} transients and tracheal filopodial extension versus
645 retraction. See source data Figure 3 - Source Data 1.
646
647 **Figure 3 - Figure Supplement 1. Distribution of microtubules and F-actin in larval**
648 **CNS trachea.**
649 (**A**) Microtubules (aTub-GFP) were present in major tracheal branches and a few
650 filopodia (arrow), but the majority of filopodia were unlabeled (asterisks). F-actin
651 (Lifeact-GFP) was found to be present in all tracheal membrane protrusions (e.g. dash
652 boxes). (**B**) Two more examples of the associated microdomain-tracheal filopodia
653 retraction events. Note that tracheal filopodia (arrows) entered microdomains that
654 reached their peak (dash lines). (**C**) Distribution of onset of filopodial extension or
655 retraction events relative to astrocyte microdomain Ca^{2+} peaks. Compared to retraction
656 onset, the onset of extension time is more broadly distributed relative to the peak
657 astrocyte Ca^{2+} signal. (**D**) Tracheal dynamics do not correlate with astrocyte
658 microdomain Ca^{2+} transients that occur at a distance. A circle with a 7.5μm radius was
659 drawn around filopodial tips, and we attempted to correlate the onset of tracheal
660 extension or retraction with astrocyte Ca^{2+} signals. We found a lack of correlation. See
661 source data Figure 3 – Figure Supplement 1 - Source Data 2.
662
663 **Figure 4. Loss of TrpML leads to overgrowth of trachea and excessive reactive**
664 **oxygen species (ROS) in larval CNS.**
665 (**A**) Quantification of average filopodial retraction and extension rates, and maximal
666 length of tracheal filopodia (n indicate the number of filopodia randomly selected from 6-
667 8 larval CNS, mean±SEM, t-test). (**B**) Comparison of changes in extension/retraction
668 ratios after bath application of tyramine in control and *trpml*^{1} mutants (n=6, mean±SEM,

669 one-way ANOVA across groups; within groups, paired t-test). (**C**) In control, one tracheal
670 branch (labeled with *btl>myr::tdTom*, arrowhead) near the LON (Brp, blue) grows short
671 filopodia (arrows) into the LON. In *trpml*^{1}, two transverse tracheal branches grow near
672 the LON, and they exhibit increases in filopodial extension into the LON (n=20,
673 mean±SEM, t-test. scale bar, 10μm). (**D**) Dihydroethidium (DHE) staining in indicated
674 genotypes. ROS-oxidized DHE forms 2-hydroxyethidium (2-OH-E^{+}) and ethidium (E^{+}).
675 Quantifications to right (n=6, mean±SEM, t-test. scale bar, 50μm). NAC was added 5
676 min prior to DHE incubation. (**E**) Proposed model. Astrocyte microdomain Ca^{2+}
677 transients are modulated by reactive oxygen species (ROS) and TrpML. Astrocyte Ca^{2+}
678 signaling can facilitate filopodial retraction if a tracheal filopodium enters a microdomain.
679 Cell cortex underlying membrane or lysosomal localization of TrpML regulates Ca^{2+}
680 signaling in response to ROS, presumably due to increased O_2 delivery, to generate
681 astrocyte microdomain Ca^{2+} transients. Tyramine induces increased microdomain Ca^{2+}
682 transients via TrpML. Loss of astrocyte microdomains resulted from *trpml* mutation
683 leads to overgrown trachea including filopodia, and increased ROS. See source data
684 Figure 4 - Source Data 1.
685
686 **Figure 4 - Figure Supplement 1. Tracheal branches overgrow in the larval ventral**
687 **nerve cord of *trpml*^{1} mutants.**
688 (**A**) Quantification of average filopodial retraction and extension rates, and maximal
689 length of tracheal filopodia. Trachea is labeled using *btl-LexA>LexAop-rCD2RFP* (n=37-
690 69 filopodia randomly selected from 6 larval CNS in each genotype indicated,
691 mean±SEM, one-way ANOVA). (**B**) Tracheal autofluorescence when illuminated with
692 408nm laser was used to trace individual branches sprouting from the uniquely
693 identifiable pair of mpgTr (red arrows). The ventral nerve cords are outlined with red
694 dash lines (n=8-10, mean±SEM, t-test). (**C**) Schematic of larval optic neuropil (LON). ap,
695 astrocyte process; tb, tracheal branch; tf, tracheal filopodium. Representative confocal
696 images of larval brains showing the position of LONs (dash boxes). Image represents
697 an 8.1μm z-projection, covering brain neuropil and LONs (blue) and associated tracheal
698 branches/filopodia. LONs zoomed in Fig 4C. (**D**) Background fluorescence intensity in

DHE staining (n=6, mean±SEM, one-way ANOVA). See source data Figure 4 – Figure Supplement 1 - Source Data.

Figure 1 – Figure Supplement 2 – Video 1. Microdomain Ca^{2+} transients in acutely dissected CNS preparations from wildtype 3rd instar (L3) larva.

Figure 1 – Figure Supplement 3 – Video 2. Microdomain Ca^{2+} transients in intact CNS preparation from wildtype 1st instar larva.

Figure 2 - Figure supplement 2 – Video 1. Microdomain Ca^{2+} transients in acutely dissected CNS preparations from *trpml* mutant 3rd instar (L3) larva.

Figure 2 – Figure supplement 3 – Video 2. Microdomain Ca^{2+} transients pre/post H_2O_2 treatment in wild type 3rd instar (L3) larva.

Figure 2 – Figure supplement 4 – Video 3. Microdomain Ca^{2+} transients pre/post H_2O_2 treatment in *trpml*^{1} mutant 3rd instar (L3) larva.

Figure 3 – Figure supplement 2 – Video 1. Microdomain Ca^{2+} transients and tracheal filopodial dynamics in wildtype L3 CNS preparation, related to Figure 3D.

Source data

Figure 1 - Source Data 1. Characterization of microdomain Ca^{2+} transients in *Drosophila* astrocytes.

Figure 2 – Source Data 1. Astrocyte microdomain Ca^{2+} transients require TrpML.

Figure 2 - Source Data 2. Astrocyte microdomain Ca^{2+} transients are genetically distinct from soma transients and require TrpML.

Figure 3 - Source Data 1. Distribution of microtubules and F-actin in larval CNS tracheal elements.

Figure 3 - Source Data 2. Astrocyte microdomain Ca^{2+} transients are associated with tracheal branches and precede retraction onset of tracheal filopodia.
hea.

Figure 4 - Source Data 1. Loss of TrpML leads to overgrowth of trachea and excessive reactive oxygen species (ROS) in larval CNS.

Figure 4 - Source Data 2. Tracheal branches overgrow in the larval ventral nerve cord of *trpml*^{1} mutants.

Additional Source Data

Source Data 1 - Manual VS AQuA. Manual method and AQuA identify comparable amount of microdomain Ca^{2+} transients.

References

Agarwal, A., Wu, P.-H., Hughes, E. G., Fukaya, M., Tischfield, M. A., Langseth, A. J., Wirtz, D., & Bergles, D. E. (2017). Transient Opening of the Mitochondrial Permeability Transition Pore Induces Microdomain Calcium Transients in Astrocyte Processes. *Neuron*, *93*(3), 587-605.e7. https://doi.org/10.1016/j.neuron.2016.12.034

Bazargani, N., & Attwell, D. (2016). Astrocyte calcium signaling: The third wave. *Nature Neuroscience*, *19*(2), 182–189. https://doi.org/10.1038/nn.4201

Bindokas, V. P., Jordan, J., Lee, C. C., & Miller, R. J. (1996). Superoxide production in rat hippocampal neurons: Selective imaging with hydroethidine. *Journal of Neuroscience*, *16*(4), 1324–1336. https://doi.org/10.1523/JNEUROSCI.16-04-01324.1996

Cole, S. H., Carney, G. E., McClung, C. A., Willard, S. S., Taylor, B. J., & Hirsh, J. (2005). Two functional but noncomplementing Drosophila tyrosine decarboxylase genes: Distinct roles for neural tyramine and octopamine in female fertility. *The Journal of Biological Chemistry*, *280*(15), 14948–14955. https://doi.org/10.1074/jbc.M414197200

Ding, F., O'Donnell, J., Thrane, A. S., Zeppenfeld, D., Kang, H., Xie, L., Wang, F., & Nedergaard, M. (2013). A1-Adrenergic receptors mediate coordinated Ca2+ signaling of cortical astrocytes in awake, behaving mice. *Cell Calcium*, *54*(6), 387–394. https://doi.org/10.1016/j.ceca.2013.09.001

Doherty, J., Logan, M. A., Taşdemir, O. E., & Freeman, M. R. (2009). Ensheathing glia function as phagocytes in the adult Drosophila brain. *The Journal of Neuroscience: The Official Journal of the Society for Neuroscience*, *29*(15), 4768–4781. https://doi.org/10.1523/JNEUROSCI.5951-08.2009

773 Feng, X., Huang, Y., Lu, Y., Xiong, J., Wong, C.-O., Yang, P., Xia, J., Chen, D., Du, G.,
774 Venkatachalam, K., Xia, X., & Zhu, M. X. (2014). Drosophila TRPML Forms PI(3,5)P2-
775 activated Cation Channels in Both Endolysosomes and Plasma Membrane. *Journal of*
776 *Biological Chemistry*, *289*(7), 4262–4272. https://doi.org/10.1074/jbc.M113.506501
777 Freeman, M. R. (2015). Drosophila Central Nervous System Glia. *Cold Spring Harbor*
778 *Perspectives in Biology*, *7*(11). https://doi.org/10.1101/cshperspect.a020552
779 Ghabrial, A., Luschnig, S., Metzstein, M. M., & Krasnow, M. A. (2003). Branching Morphogenesis
780 of the Drosophila Tracheal System. *Annual Review of Cell and Developmental Biology*,
781 *19*(1), 623–647. https://doi.org/10.1146/annurev.cellbio.19.031403.160043
782 Im, S. H., Takle, K., Jo, J., Babcock, D. T., Ma, Z., Xiang, Y., & Galko, M. J. (2015). Tachykinin acts
783 upstream of autocrine Hedgehog signaling during nociceptive sensitization in Drosophila.
784 *ELife*, *4*, e10735. https://doi.org/10.7554/eLife.10735
785 Khakh, B. S., & McCarthy, K. D. (2015). Astrocyte calcium signaling: From observations to
786 functions and the challenges therein. *Cold Spring Harbor Perspectives in Biology*, *7*(4),
787 a020404. https://doi.org/10.1101/cshperspect.a020404
788 Kim, J., Chung, Y. D., Park, D., Choi, S., Shin, D. W., Soh, H., Lee, H. W., Son, W., Yim, J., Park, C.-
789 S., Kernan, M. J., & Kim, C. (2003). A TRPV family ion channel required for hearing in
790 Drosophila. *Nature*, *424*(6944), 81–84. https://doi.org/10.1038/nature01733
791 Kim, S. H., Lee, Y., Akitake, B., Woodward, O. M., Guggino, W. B., & Montell, C. (2010).
792 Drosophila TRPA1 channel mediates chemical avoidance in gustatory receptor neurons.
793 *Proceedings of the National Academy of Sciences*, *107*(18), 8440–8445.
794 https://doi.org/10.1073/pnas.1001425107

Ma, Z., Stork, T., Bergles, D. E., & Freeman, M. R. (2016). Neuromodulators signal through astrocytes to alter neural circuit activity and behaviour. *Nature*, *539*(7629), 428–432. https://doi.org/10.1038/nature20145

Monastirioti, M., Linn, C. E., & White, K. (1996). Characterization of Drosophila tyramine beta-hydroxylase gene and isolation of mutant flies lacking octopamine. *The Journal of Neuroscience: The Official Journal of the Society for Neuroscience*, *16*(12), 3900–3911.

Nagaya, Y., Kutsukake, M., Chigusa, S. I., & Komatsu, A. (2002). A trace amine, tyramine, functions as a neuromodulator in Drosophila melanogaster. *Neuroscience Letters*, *329*(3), 324–328. https://doi.org/10.1016/S0304-3940(02)00596-7

Nett, W. J., Oloff, S. H., & McCarthy, K. D. (2002). Hippocampal astrocytes in situ exhibit calcium oscillations that occur independent of neuronal activity. *Journal of Neurophysiology*, *87*(1), 528–537. https://doi.org/10.1152/jn.00268.2001

Paukert, M., Agarwal, A., Cha, J., Doze, V. A., Kang, J. U., & Bergles, D. E. (2014). Norepinephrine controls astroglial responsiveness to local circuit activity. *Neuron*, *82*(6), 1263–1270. https://doi.org/10.1016/j.neuron.2014.04.038

Roy, S., Huang, H., Liu, S., & Kornberg, T. B. (2014). Cytoneme-Mediated Contact-Dependent Transport of the Drosophila Decapentaplegic Signaling Protein. *Science*, *343*(6173). https://doi.org/10.1126/science.1244624

Rungta, R. L., Bernier, L.-P., Dissing-Olesen, L., Groten, C. J., LeDue, J. M., Ko, R., Drissler, S., & MacVicar, B. A. (2016). Ca2+ transients in astrocyte fine processes occur via Ca2+ influx in the adult mouse hippocampus. *Glia*, *64*(12), 2093–2103. https://doi.org/10.1002/glia.23042

817 Shigetomi, E., Jackson-Weaver, O., Huckstepp, R. T., O'Dell, T. J., & Khakh, B. S. (2013). TRPA1
818 channels are regulators of astrocyte basal calcium levels and long-term potentiation via
819 constitutive D-serine release. *The Journal of Neuroscience: The Official Journal of the*
820 *Society for Neuroscience*, *33*(24), 10143–10153.
821 https://doi.org/10.1523/JNEUROSCI.5779-12.2013
822 Shigetomi, E., Tong, X., Kwan, K. Y., Corey, D. P., & Khakh, B. S. (2011). TRPA1 channels regulate
823 astrocyte resting calcium and inhibitory synapse efficacy through GAT-3. *Nature*
824 *Neuroscience*, *15*(1), 70–80. https://doi.org/10.1038/nn.3000
825 Sprecher, S. G., Cardona, A., & Hartenstein, V. (2011). The Drosophila larval visual system: High-
826 resolution analysis of a simple visual neuropil. *Developmental Biology*, *358*(1).
827 https://doi.org/10.1016/j.ydbio.2011.07.006
828 Srinivasan, R., Huang, B. S., Venugopal, S., Johnston, A. D., Chai, H., Zeng, H., Golshani, P., &
829 Khakh, B. S. (2015). Ca(2+) signaling in astrocytes from Ip3r2(-/-) mice in brain slices and
830 during startle responses in vivo. *Nature Neuroscience*, *18*(5), 708–717.
831 https://doi.org/10.1038/nn.4001
832 Stork, T., Sheehan, A., Tasdemir-Yilmaz, O. E., & Freeman, M. R. (2014). Neuron-glia interactions
833 through the Heartless FGF receptor signaling pathway mediate morphogenesis of
834 Drosophila astrocytes. *Neuron*, *83*(2), 388–403.
835 https://doi.org/10.1016/j.neuron.2014.06.026
836 Venkatachalam, K., Long, A. A., Elsaesser, R., Nikolaeva, D., Broadie, K., & Montell, C. (2008).
837 Motor Deficit in a Drosophila Model of Mucolipidosis Type IV due to Defective Clearance
838 of Apoptotic Cells. *Cell*, *135*(5), 838–851. https://doi.org/10.1016/j.cell.2008.09.041

839 Walker, R. G., Willingham, A. T., & Zuker, C. S. (2000). A Drosophila Mechanosensory
840 Transduction Channel. *Science*, *287*(5461), 2229–2234.
841 https://doi.org/10.1126/science.287.5461.2229
842 Wang, Y., DelRosso, N. V., Vaidyanathan, T. V., Cahill, M. K., Reitman, M. E., Pittolo, S., Mi, X., Yu,
843 G., & Poskanzer, K. E. (2019). Accurate quantification of astrocyte and neurotransmitter
844 fluorescence dynamics for single-cell and population-level physiology. *Nature*
845 *Neuroscience*, *22*(11), 1936–1944. https://doi.org/10.1038/s41593-019-0492-2
846 Wong, C.-O., Gregory, S., Hu, H., Chao, Y., Sepúlveda, V. E., He, Y., Li-Kroeger, D., Goldman, W.
847 E., Bellen, H. J., & Venkatachalam, K. (2017). Lysosomal Degradation Is Required for
848 Sustained Phagocytosis of Bacteria by Macrophages. *Cell Host & Microbe*, *21*(6), 719-
849 730.e6. https://doi.org/10.1016/j.chom.2017.05.002
850 Zhang, X., Cheng, X., Yu, L., Yang, J., Calvo, R., Patnaik, S., Hu, X., Gao, Q., Yang, M., Lawas, M.,
851 Delling, M., Marugan, J., Ferrer, M., & Xu, H. (2016). MCOLN1 is a ROS sensor in
852 lysosomes that regulates autophagy. *Nature Communications*, *7*, 12109.
853 https://doi.org/10.1038/ncomms12109
854 Zhang, Y. V., Ormerod, K. G., & Littleton, J. T. (2017). Astrocyte Ca2+ Influx Negatively Regulates
855 Neuronal Activity. *ENeuro*, *4*(2). https://doi.org/10.1523/ENEURO.0340-16.2017
856

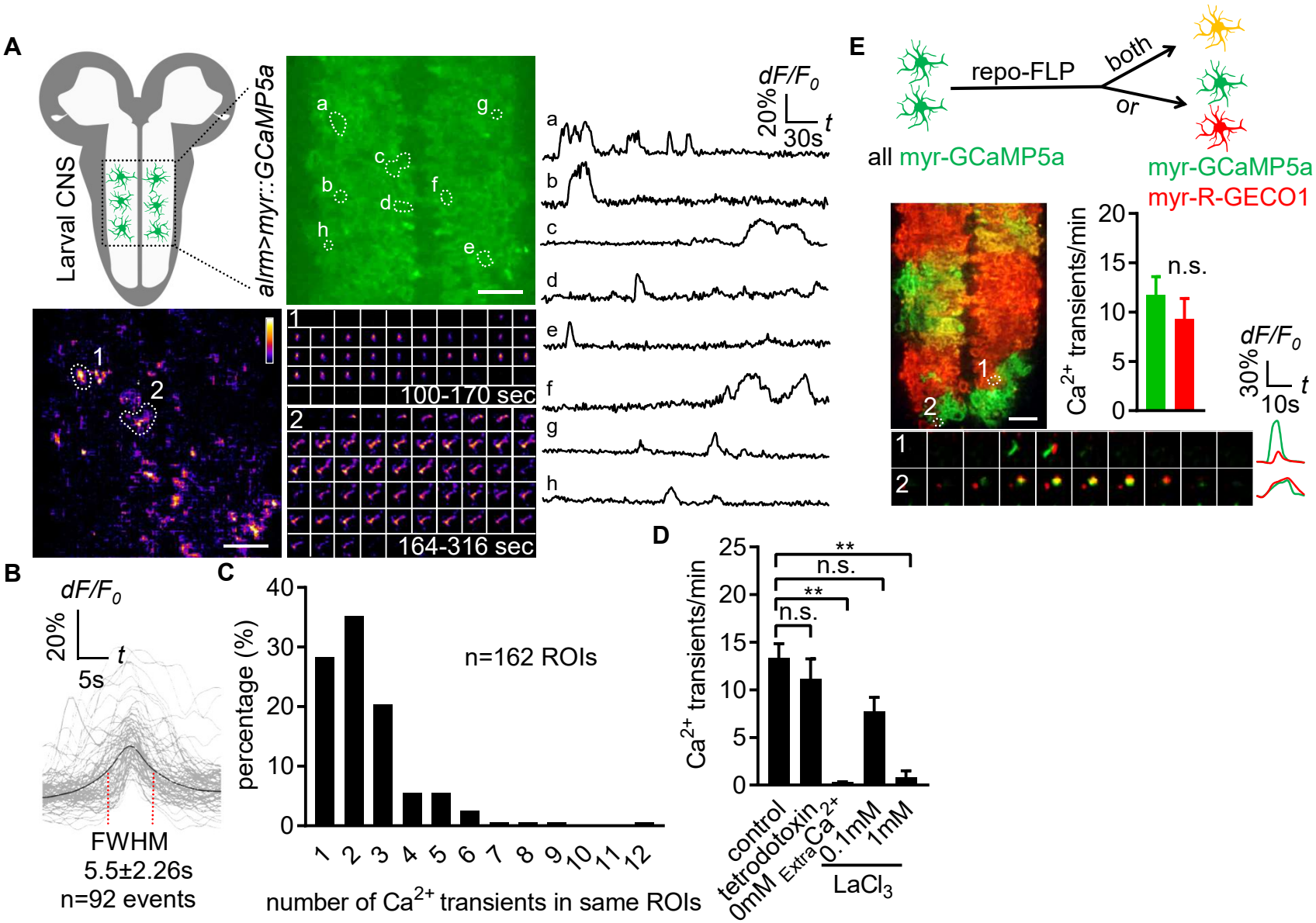

Fig. 1 Ma & Freeman 2020

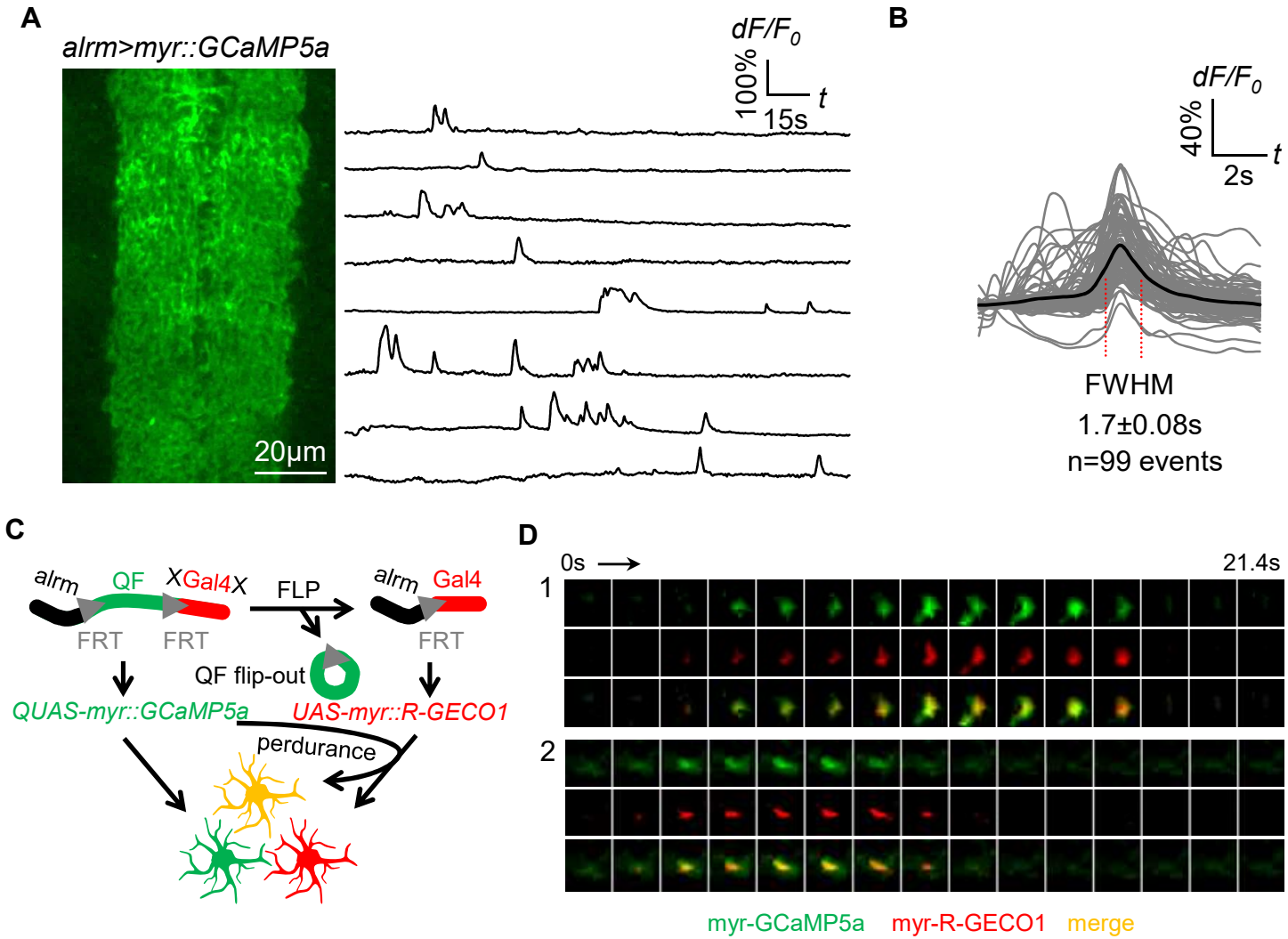

Fig. 1-Fig. Supp. 1 Ma & Freeman 2020

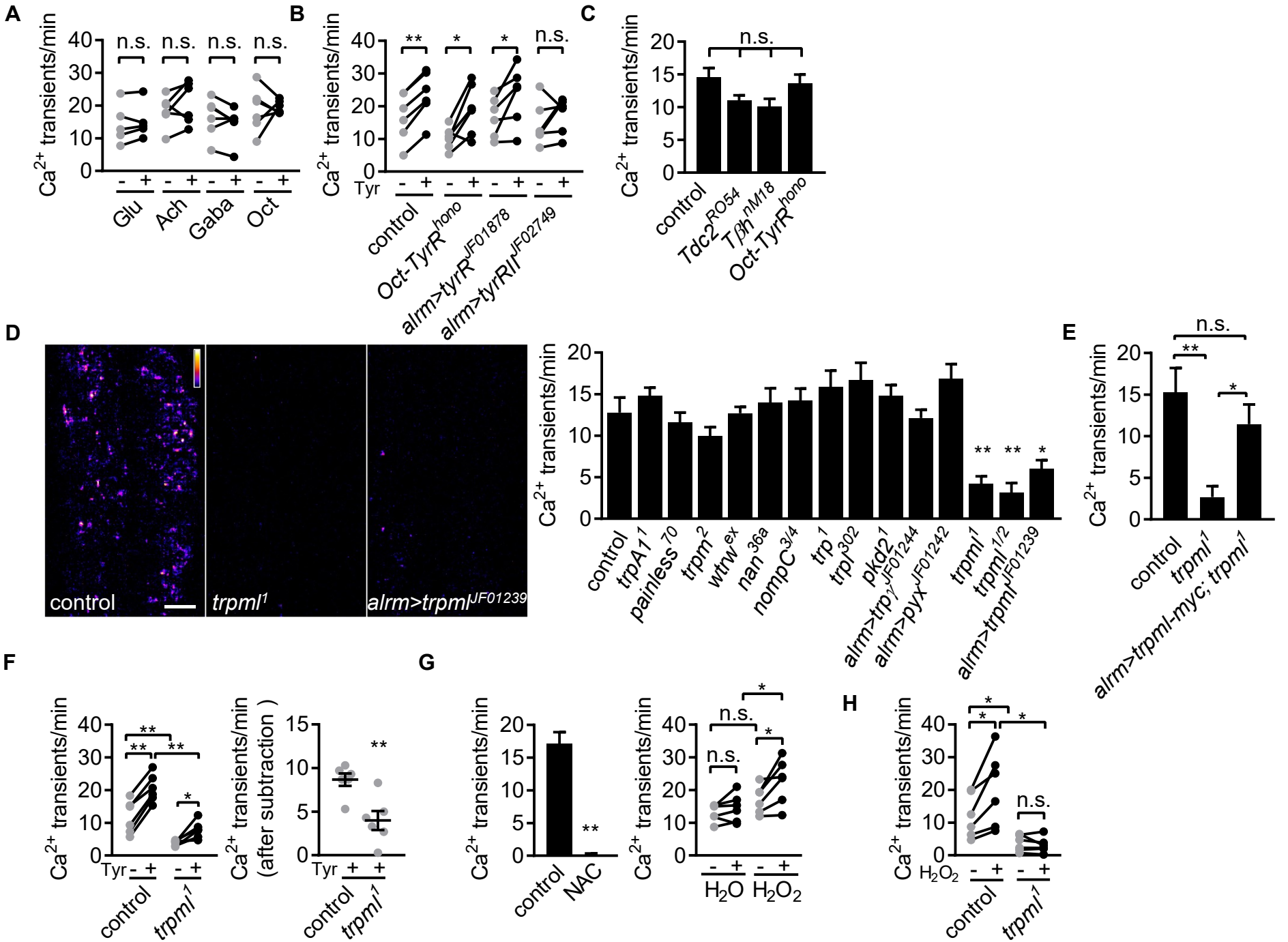

Fig. 2 Ma & Freeman 2020

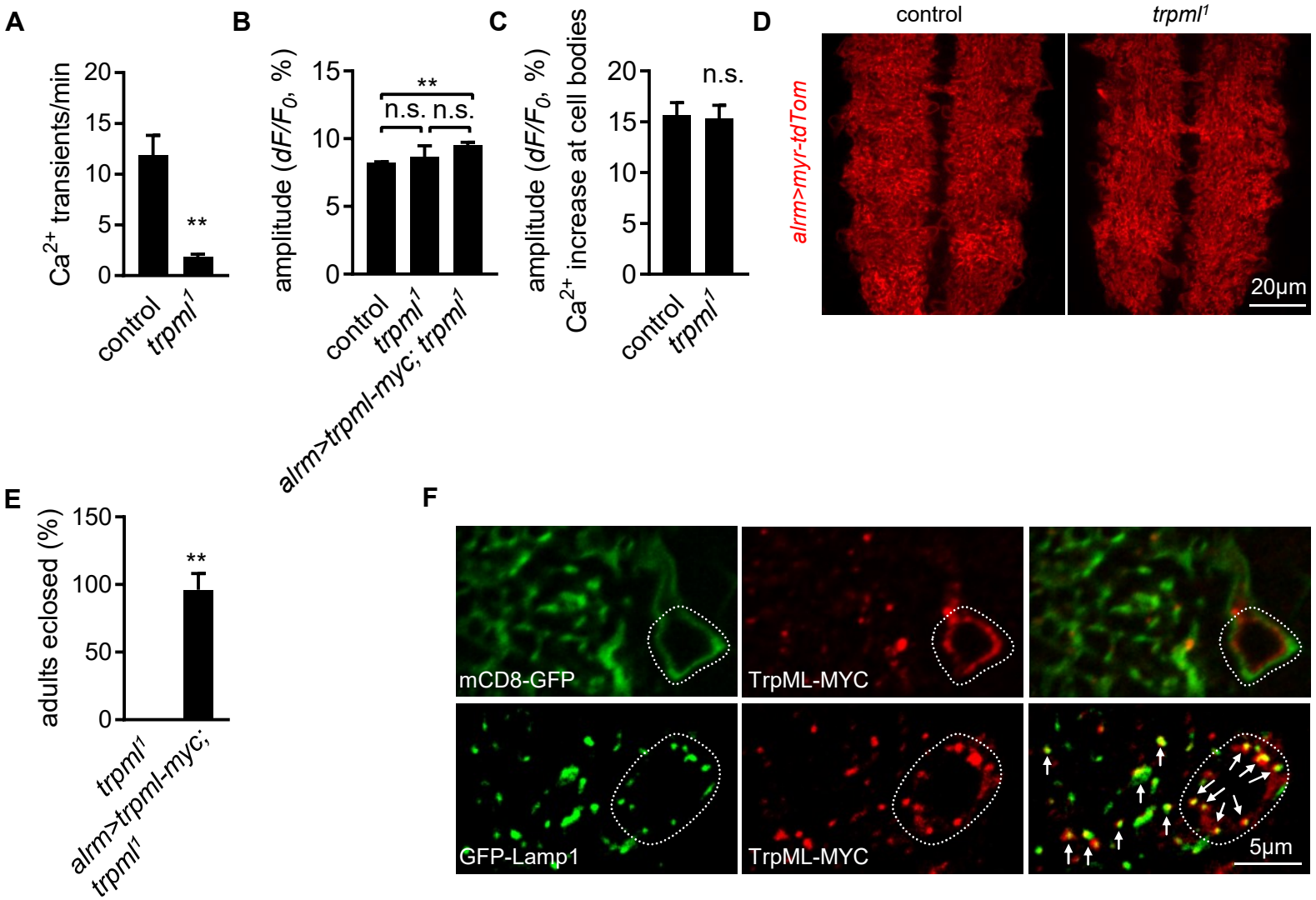

Fig. 2-Fig. Supp. 1 Ma & Freeman 2020

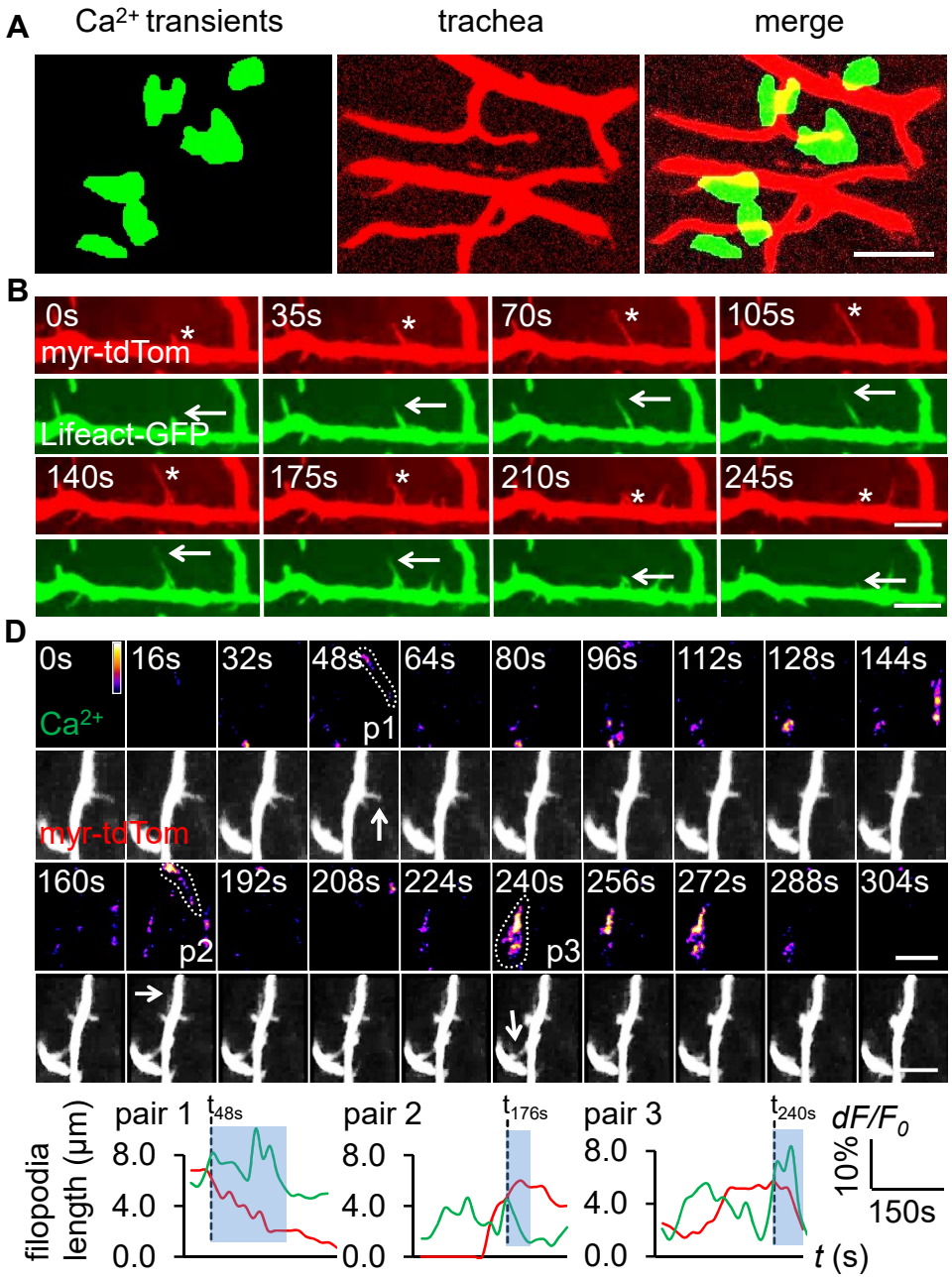

C

Type	w/ Ca^{2+}	w/o Ca^{2+}
Extension (3)	1	2
Retraction (36)	26	10
Extension & Retraction (131)	61	70
Stationary (4)	2	2
Total (174)	90	84

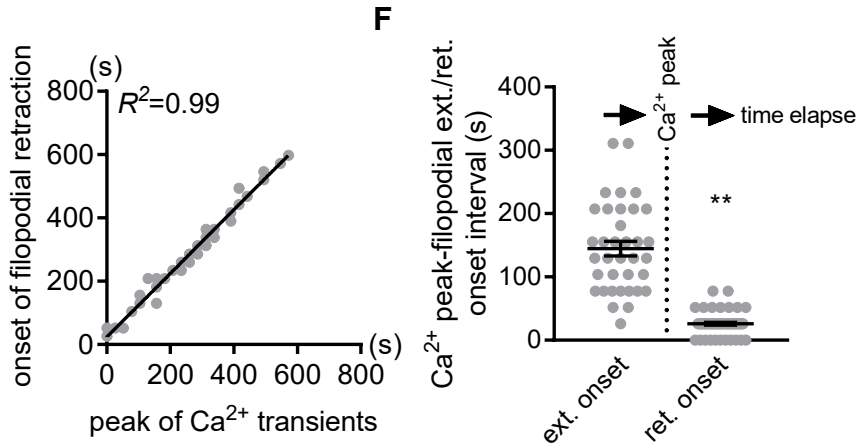

Fig. 3 Ma & Freeman 2020

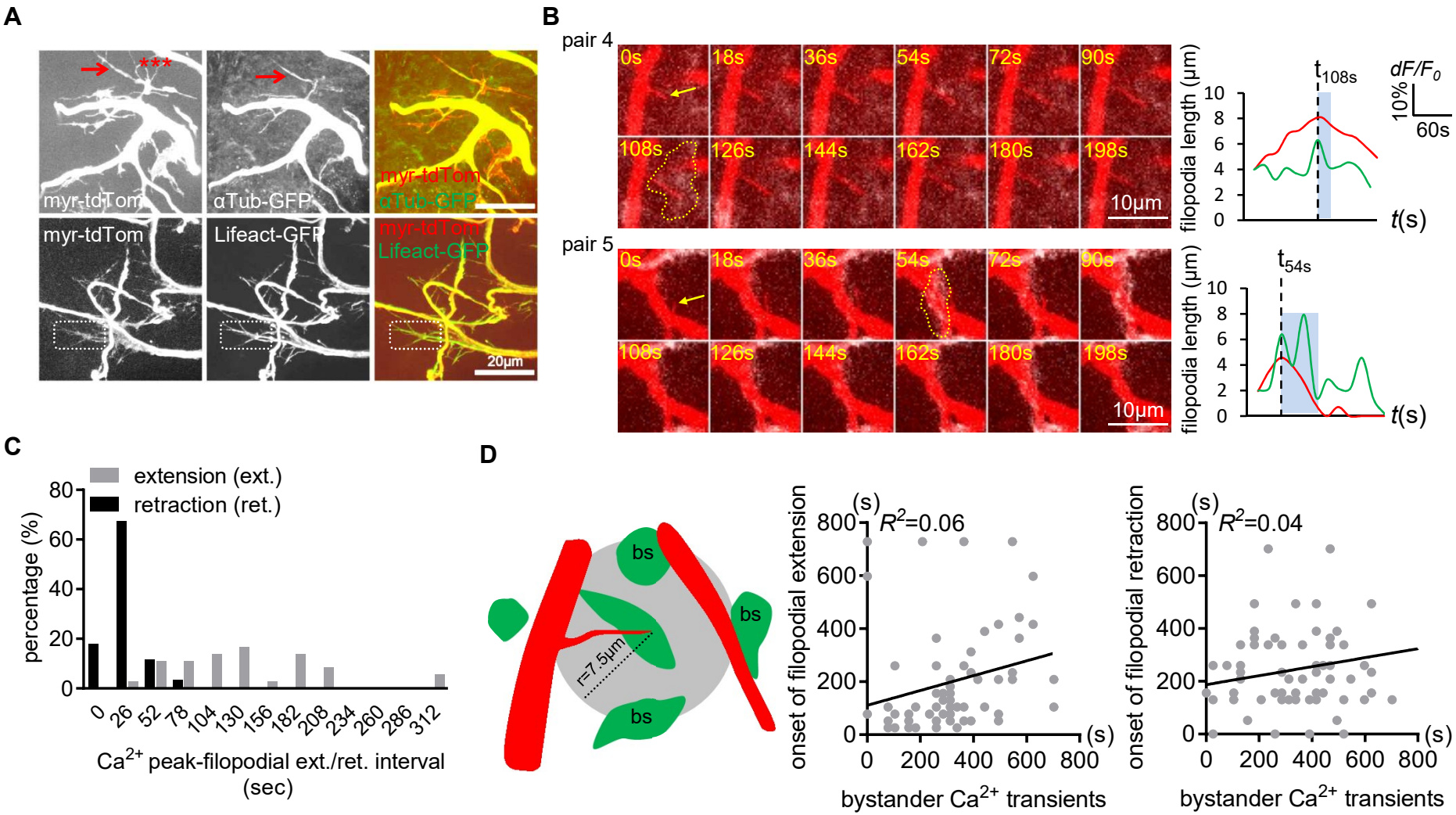

Fig. 3-Fig. Supp. 1 Ma & Freeman 2020

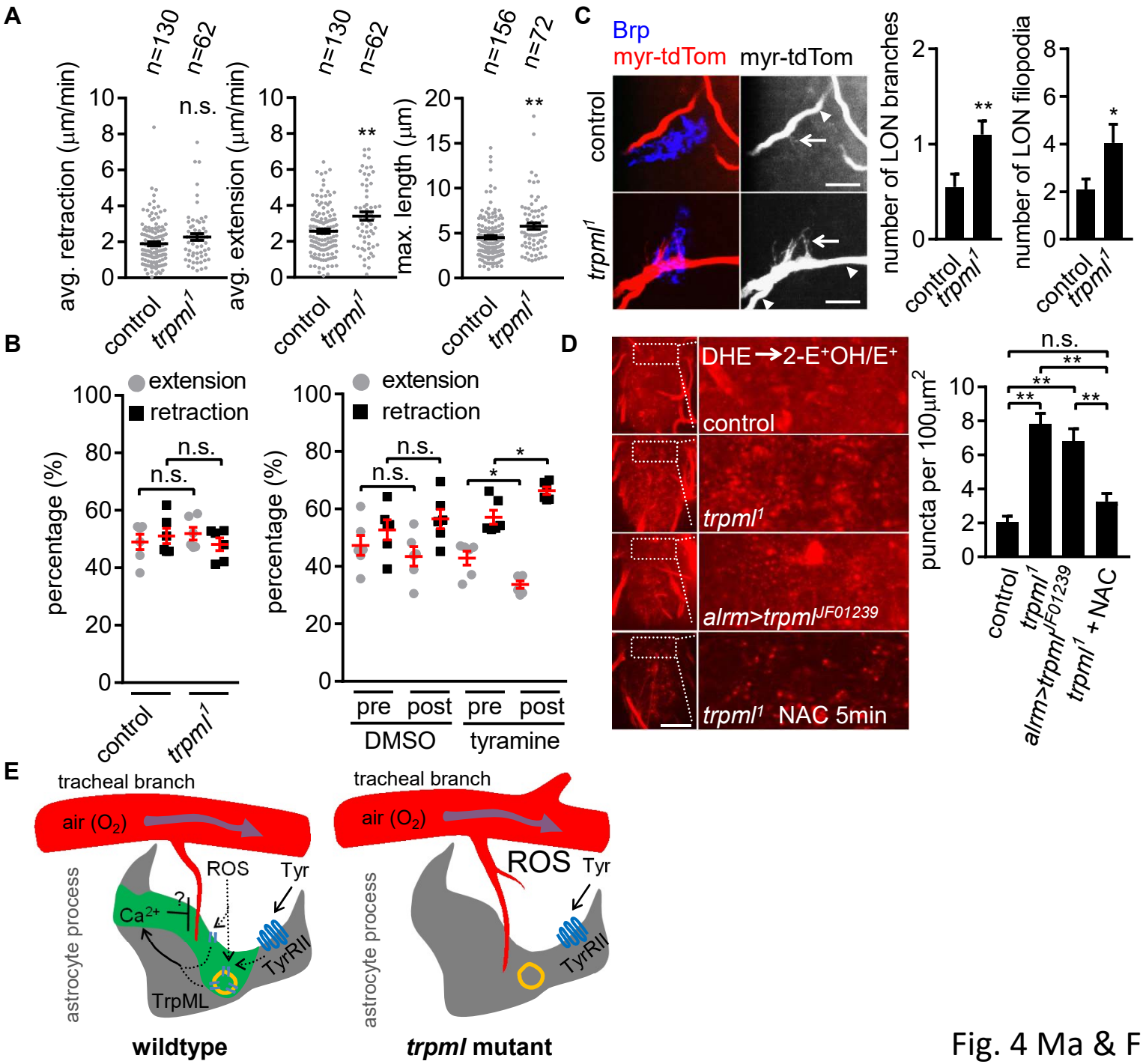

Fig. 4 Ma & Freeman 2020

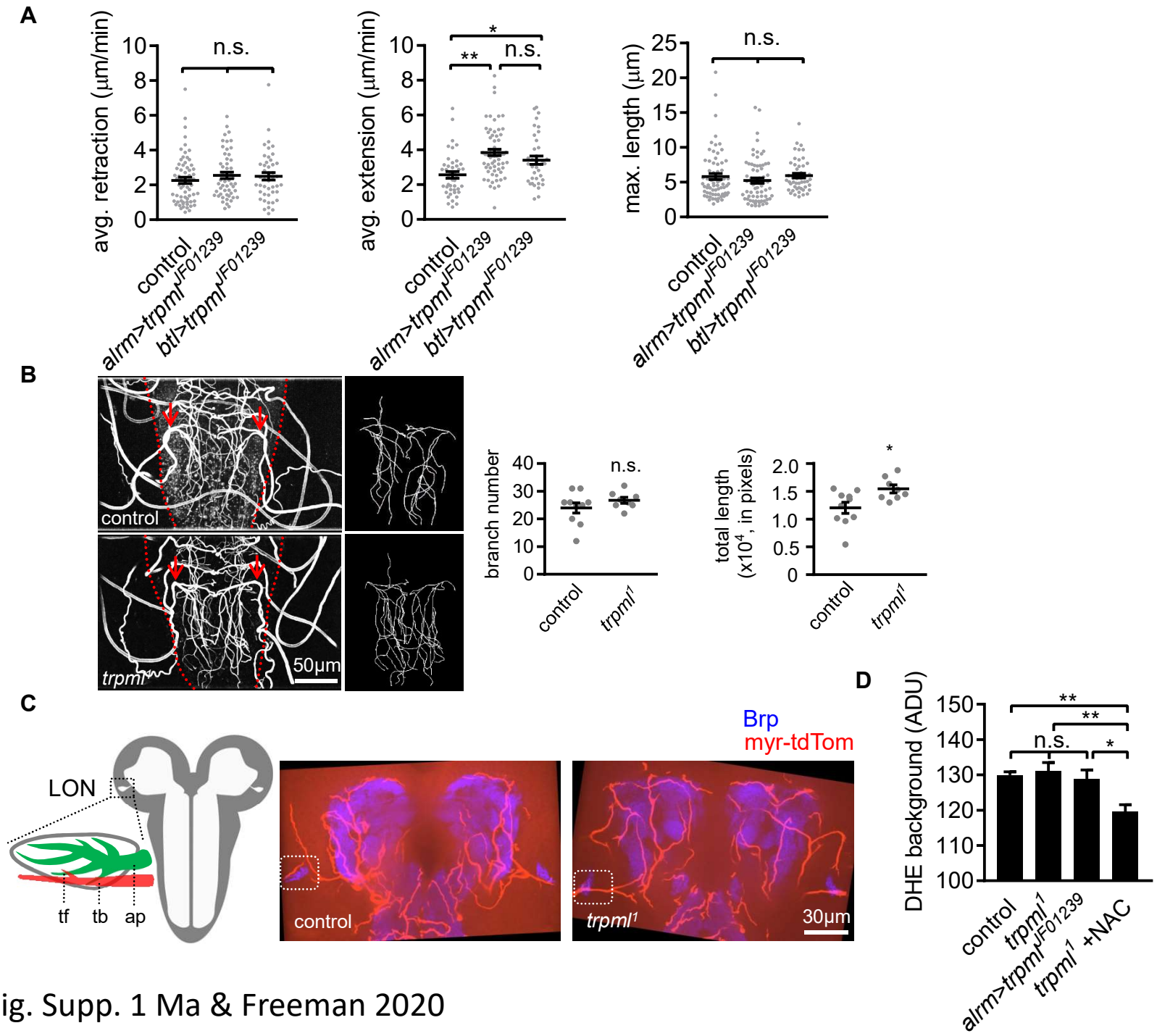

Fig. 4-Fig. Supp. 1 Ma & Freeman 2020